NOVA SCHOOL OF SCIENCE & TECHNOLOGY

DEPARTAMENT OF MATERIALS SCIENCE

Gabriel Barbosa Félix

BSc in Micro and Nanotechnology Engineering

PRODUCTION AND ELECTRICAL CHARACTERISATION OF MICROSENSORS FOR MARINE MUTAGENS AND CARCINOGENS MONITORING

MASTER IN MICRO AND NANOTECHNOLOGY ENGINEERING

NOVA University Lisbon

September, 2022

DEPARTAMENT OF
MATERIALS SCIENCE

NOVA SCHOOL OF
SCIENCE & TECHNOLOGY

PRODUCTION AND ELECTRICAL CHARACTERISATION OF MICROSENSORS FOR MARINE MUTAGENS AND CARCINOGENS MONITORING

GABRIEL BARBOSA FÉLIX

BSc in Micro and Nanotechnology Engineering

Adviser: Dr. Pedro Miguel Cândido Barquinha
Associate Professor, FCT NOVA University Lisbon, Materials Science Department

Co-adviser: Dr. Bruno Miguel Ribeiro Veigas
Senior Researcher, Almascience

Examination Committee:

Chair: Dr. Rui Alberto Garção Barreira do Nascimento Igreja
Assistant Professor, NOVA University Lisbon

Rapporteurs: Dr. Rita Maria Mourão Salazar Branquinho
Associate Professor, NOVA University Lisbon

Adviser: Dr. Bruno Miguel Ribeiro Veigas
Senior Researcher, Almascience

MASTER IN MICRO AND NANOTECHNOLOGY ENGINEERING

NOVA University Lisbon
SEPTEMBER, 2022

Production and electrical characterization of microsensors for marine mutagens and carcinogens monitoring

Acknowledgments

Começo por agradecer a toda a gente envolvida no DCM, CENIMAT e CEMOP e todos os que tomaram parte no processo pedagógico do MIEMN, ao Professor Rodrigo Martins e Professora Elvira Fortunato por terem criado este curso único no país, com o qual me fui identificando cada vez mais ao longo de 5 anos.

A special acknowledgement goes to everyone involved in the project SeaSenseX (MACAU/0022019), for allowing to develop my master thesis around this project. I had the pleasure of working with you, always having in mind that this work had a bigger purpose than just an academic master thesis. It was a pleasure to integrate a collective work to help fixing a real problem in the world we live in.

Este final de percurso de mestrado não teria sido possível sem a contribuição de certas pessoas. Começo por agradecer ao meu orientador, o Professor Pedro Barquinha. Foi um dos melhores professores que tive durante o meu percurso académico. Admiro a sua vontade e boa disposição na forma como nos transmitiu o seu conhecimento, sempre de forma interativa e clara. Ao meu co-orientador, Bruno Veigas, que esteve sempre disponível, elevando o meu espírito crítico para avaliar os frutos do meu trabalho e apresentá-los da melhor forma possível. Mostrou-me também como encarar as coisas com mais objetividade e tranquilidade. Não podia deixar de agradecer à Professora Joana Pinto, que foi incansável e esteve presente desde o início para me assistir com todas as questões e me ajudou a encontrar soluções para tudo o que foi aparecendo pela frente. Ao Pedro, Bruno e Joana, ficarei sempre grato pela oportunidade e confiança que criaram para eu desenvolver este trabalho. À Inês Santos, obrigado por toda a disponibilidade em ser a minha mentora de câmara limpa e criar condições para o meu trabalho experimental ser desenvolvido.

Aos restantes professores que fizeram parte do meu percurso académico, destaco a influência da Professora Rita Branquinho que com a sua fantástica pedagogia, fomentou o meu interesse no mundo da nanotecnologia. Ao Professor Luís Pereira por ter tido sempre a maior paciência e disponibilidade para explicar e arranjar formas para tornar simples aquilo que parecia complicado no mundo da micro e optoelectrónica.

Um agradecimento especial aos meus pais. Mãe por seres sem dúvida a pessoa que mais perto de mim esteve em toda a minha vivência, que me deu sempre o maior carinho e atenção. Pai, apesar de muitas vezes fisicamente longe, quando estás presente sei que tentas sempre dar-me o melhor de ti, e ensinar-me com piadas e boa disposição. Eu sei que ambos sempre fizeram por me dar o melhor de vocês, proporcionaram-me uma infância e adolescência bastante felizes, que me levaram a conhecer os cantos do mundo, dando-me sempre o vosso amor. Ao meu gato, Quickie, desde os meus 10 anos até agora... sempre me proporcionou felicidade. Quando estava mal… em baixo, revoltado com coisas da vida… era quem eu tinha sempre para me fazer companhia e me dar amor de uma forma que não dá para explicar. A toda a minha família, aos presentes e aos que já partiram, todos sabem o quão importantes são para mim. Um foco especial na minha avó Lélé, será sempre das mulheres mais importantes da minha vida, por quem tenho uma consideração e carinho maior do que este mundo, por tudo o que fez por mim, por todos os bons momentos e memórias felizes. À minha namorada, Marta, MJ, uma das pessoas mais importantes da minha vida, que conheci no início deste percurso de faculdade. Das pessoas mais maravilhosas que conheço… é acima de tudo a minha melhor amiga e está disponível para tudo e mais alguma coisa sem exceção, não tenho palavras para expressar o quão importante és para mim.

Finalmente aos amigos, a quem devo muito por todos os momentos e memórias, Manel, Tomás, Rui, Marco, Carvalho, João Rosbife, Mateus, Santos, Filipe, Diogo, Vitinho, Ana, Larissa, Quary, Soko, Horta, Gonçalo, Almeida, Ane, Vitória, Mariana, Sofia… e outros tantos, vocês foram, são, serão pessoas que contribuem para grande parte da minha felicidade.

“I, a universe of atoms, an atom in the universe.”

Richard P. Feynman

Abstract

Field effect-based devices (FED) show several advantages when implemented as biosensors, such as small dimensions, fast response, low-cost mass production and easy integration with CMOS or TFT technologies. However, conventional architectures have some inherent drawbacks that hinder further miniaturisation. Recently, a charge-modulated field-effect transistor (CMFET) architecture has been developed, following the operation principle of the floating-gate transistor, used in memory devices, having a control-gate functioning as reference electrode and a sensing area activated by charge induction, which modulates the channel of an integrated MOS transistor. This work focuses on the development and optimization of CMFET sensor architecture produced for the first time on eco-friendly and flexible paper substrates. The performance of these paper based CMFETS was then compared with the previously developed sensors produced on substrates such as Corning glass and polyethylene naphthalate (PEN), which shared an identical fabrication process already established at CENIMAT|I3N. Measurement and analysis protocols were created and optimized to assess the sensors' performance and establish a comprehensive comparison between sensors fabricated on different substrates. Furthermore, an alternative connecting topology was tested for the developed charge-modulated field-effect sensing architecture, with results of sensitivity scaling up to 300% relative to the values obtained with the standard connecting topology, identical to the ones reported in the literature. Although it was not possible to attain a batch of devices without considerable variability in capacitance, sensors on paper substrates were capable of outputting distinct current levels for each pH buffer solution tested (7, 4 and 10) exhibiting a sensitivity of 14 ± 2 mV/pH (Whatman paper) and 32 ± 6 mV/pH (CelSmartSense paper), relative to 33 ± 3 mV/pH obtained for sensors produced on Corning glass and 28 ± 2 mV/pH for sensors on PEN substrate, improving the sensitivity and signal to noise ratio previously reported for this architecture.

Keywords: field effect; pH sensor, cellulose-based, eco-friendly, flexible substrate

Resumo

Dispositivos baseados em efeito de campo (FED) apresentam inúmeras vantagens quando implementados como biossensores, entre as quais, reduzidas dimensões, resposta rápida, produção em massa de baixo custo e fácil integração com tecnologias CMOS ou TFT. No entanto, as arquiteturas mais comuns apresentam algumas desvantagens que criam uma barreira ao processo de miniaturização. Recentemente foi desenvolvida uma arquitetura sensorial baseada em modulação de cargas por efeito de campo (CMFET), que segue o princípio de operação do transístor de porta flutuante, utilizado em dispositivos de memória, fazendo uso de um elétrodo de controlo e uma área sensível ativada por indução de cargas, que modula o canal de condução de um transístor MOS integrado. Este trabalho foca o desenvolvimento e caracterização elétrica de sensores baseados na arquitetura CMFET em substratos de papel ecológicos e flexíveis. A performance destes sensores foi por sua vez comparada com sensores fabricados substratos de referência como vidro *Corning* e naftalato de polietileno (PEN), que partilharam um processo de fabricação idêntico, já estabelecido no CENIMAT|I3N. Protocolos de medição e análise foram criados e otimizados para comparar o desempenho dos sensores fabricados em diferentes substratos. Além disto, um esquema de conexão alternativo foi testado para esta arquitetura de sensores, exibindo resultados de sensibilidade que escalaram 300% face a resultados testados com a conexão standard, idênticos aos reportados na literatura. Embora não tenha sido possível produzir lotes de dispositivos sem uma variabilidade considerável na sua capacitância, os sensores fabricados foram capazes de produzir níveis de corrente distintos para cada pH testado (4,7 e 10), exibindo uma sensibilidade de 14 ± 2 mV/pH (papel Whatman) e 32 ± 6 mV/pH (papel CelSmartSense), em relação a 33 ± 3 mV/pH, valor obtido com sensores produzidos em vidro *corning* e 28 ± 2 mV/pH para sensores produzidos em substrato de PEN, melhorando a sensibilidade conseguida anteriormente com esta arquitetura.

Palavras chave: efeito de campo; sensor de pH, celulose, ecológico, substratos flexíveis

Table of Contents

List of Figures

List of Tables

Acronyms

CEMOP	Centre of Excellence in Microelectronics Optoelectronics and Processes
CENIMAT	Centro de Investigação de Materiais
CMFET	Charge-modulated field-effect transistor
CMISFET	Charge-modulated ion sensitive field-effect transistor
CMOS	Complementary metal-oxide-semiconductor
C-V	Capacitance-voltage
CVD	Chemical vapor deposition
EIS	Electrolyte-insulator-semiconductor
FED	Field-effect device
FET	Field-effect transistor
IC	Integrated circuit
ISFET	Ion sensitive field-effect transistor
LPCVD	Low power chemical vapor deposition
MIS	Metal-insulator-semiconductor
MOSFET	Metal-oxide-semiconductor field-effect transistor
PEN	Polyethylene naphthalate
PECVD	Plasma enhanced chemical vapor deposition
PVD	Physical vapor deposition
RF	Radio frequency
RT	Real time
SER	Signal to error ratio
SMU	Source measure unit
TFT	Thin film transistor
UN	United Nations

ZIF	Zero insertion force

Symbols

A	Area
C	Capacitance
C_{dif}	Electrolyte differential capacitance
I_D	Drain current
I_{DS}	Drain-to-source current
k_B	Boltzmann constant
p-Si	p-type doped silicon
$\mathbf{pH}_{pzc}$	Point of zero charge
q	Electron charge
Q_S	Surface charge
T	Temperature
V	Voltage
V_C	Control voltage
V_{GS}	Gate-to-source voltage
V_{TH}	Threshold voltage
V_{Ref}	Reference voltage
α	Oxide sensitivity parameter
β_{int}	Oxide intrinsic buffer capacity
ε_0	Vacuum permittivity
ε_r	Dielectric constant/Relative dielectric permittivity
λ_D	Debye length
ψ	Surface potential

1 Motivation and objectives

Over the last decades domestic and industrial wastes have seen an exponential growth, resulting in thousands of chemical substances being disposed and released to the environment. Pollution of oceans and rivers has caused a severe impact on wildlife, leaving a threat to thousands of organisms who are not able to adapt to the rising levels of toxicity. With this problematic in mind and under the ambitious Goal 14 of UN's 2030 Agenda, conservation of the seas calls for innovative technologies for monitoring marine pollutants accurately, reproducibly, and affordably.

The present work is part of project SeaSenseX "Next-generation microsensors for marine mutagens and carcinogens" which is a collaboration between FCT-NOVA and University of Macau that seeks to address the mentioned problematic through the design of a sensing platform based on a multifactorial chip-based technology. It envisions the development of a novel, reliable and inexpensive process for monitoring potential mutagens and carcinogens in marine environments through the characterization of key biomarkers.

This MSc work focuses on the production and electrical characterization of CMISFET sensors on several substrates in order to assess their ability to output an accurate signal according to the medium they are exposed to, and in the end establish a comparison between substrates while establishing a direct comparison to state-of-the-art devices in this category. Moreover, cellulose-based substrates were introduced for the first time for this sensor architecture in order to assess if the performance could match the one of glass or PEN, bringing the advantage of having a more eco-friendly and altogether less expensive device.

The first task of this work is the production of sensors on different substrates in clean room with the use of physical masks already fabricated according to a previous study of CMISFET sensors architecture, design and optimization. Following that, electrical characterisation of the sensors to do a comparison study of sensors on different substrates, was performed. This includes preliminary capacitance tests (CV curves) and the development and optimization of the measurement and data analysis protocol for this sensing architecture, to allows a comprehensive comparison of sensors produced on different substrates.

This work was financed by national funds from FCT - Fundação para a Ciência e a Tecnologia, I.P., in the scope of the projects LA/P/0037/2020, UIDP/50025/2020 and UIDB/50025/2020 of the Associate Laboratory Institute of Nanostructures, Nanomodelling and Nanofabrication – i3N, as well as through the projects MACAU/0002/2019 (SeaSenseX) and PTDC/CTM-PAM/4241/2020 (IDS-Paper). The work was also funded by the European Community's H2020 program under grant agreements No. 952169 (SYNERGY, H2020-WIDESPREAD-2020-5, CSA) and No. 101008701 (EMERGE, H2020-INFRAIA-2020-1).

2 Introduction

As of today, biosensors represent a wide and well-established field which continues to attract high investments, with global market analysis reporting a substantial growth over the last five years and further growth expected for the next decade [1], being domestic health monitoring a huge contribution for these devices dominance. Accompanying this growth, a similar development can be expected in various fields such as food and environmental monitoring, and biomedical areas of pathogen identification or drug screening [2]. Amongst the various biosensing platforms, field effect devices (FED) for biological detection have risen in recent years, with a great emphasis on one architecture – the field effect transistor (FET), which comes as one of the most promising approaches for bio-electrical detection and characterization. Field effect transistor based solid state sensors have attracted considerable attention since the late 1960s, immediately right after the introduction of standard silicon planar technology for integrated circuits (IC). This device architecture features several advantages such as fast response to a wide variety of stimuli, small dimensions, possibility of integration into arrays, make feasible the on-chip integration and opens a gate for low-cost mass production of devices that can be interfaced with backend electronics and computers to enable remote monitoring of desired parameters (health, environment, etc.) [3].

2.1 Field effect biosensing architectures

Field effect-based sensors mainly follow two architectures: a metal-insulator-semiconductor (MIS) capacitor and a metal-oxide-semiconductor field effect transistor (MOSFET). Over the years, these architectures have been modified to surpass the challenges and needs of integrating biological reactions with electronic devices [4]. The MIS capacitor is a remarkable device with a simple structure comprising a semiconductor-insulator interface which serves as a model for the development of sensitive layers and/or materials. The electrolyte-insulator-semiconductor (EIS) structure (Figure 2.1 A) emerged from the later, as a modified design that has been broadly applied for biosensing. Here the gate electrode is replaced by an electrolyte and a reference electrode. The insulator, typically an oxide, is directly in contact with the electrolyte, thus modulation of the device's response is achieved by a change in the oxide's surface potential, which is promoted by changes in the solution. Similarly, from the MOSFET structure, the ion sensitive field effect transistor (ISFET) sensor structure appeared, sharing a similar operation principle in its core. As in the EIS structure, the gate electrode is replaced with an electrolyte and a reference electrode, leaving the gate dielectric directly exposed to the electrolyte (Figure 2.1 B) [5].

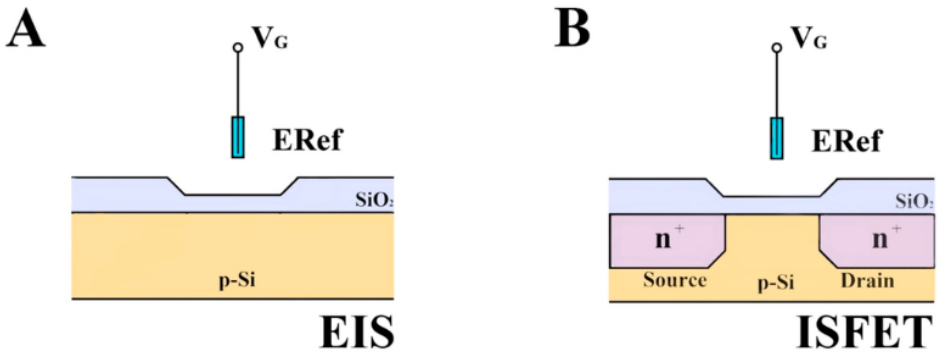

Figure 2.1 - Schematic illustration of thin film device structures: (A) EIS—electrolyte-insulator-semiconductor; (B) ISFET- ion sensitive field effect transistor; (C) CMFET—charge modulated field effect transistor. ERef: reference electrode; Vg: gate voltage; Vc: Capacitor voltage. Adapted from [6].

As of today, among the wide variety of FET solid-state sensors, ion sensitive field-effect transistor stands out as one of the most popular categories of electrical biosensors. This architecture was proposed in 1970 [7], as a pH sensor that allowed detection and quantification of ions (H+), therefore could be sensitive to chemicals through the surface of inorganic insulators while having the amplifying characteristic of the field-effect transistor. This proof of concept later led to the introduction of the first miniaturized silicon-based chemical sensor. ISFET are commonly used for pH detection that is needed in a wide range of applications, such as DNA detection and amplification [6,8], tissue health monitoring [9], bacterial and yeast growth identification [10,11], or soil and water content analysis [12,13]. They can also be modified or functionalized for potentiometric biochemical sensing of inorganic ions and biomolecules such as Na^+, K^+, Ca^{2+} [14,15]. Apart from all the advantages of FET-based devices ISFET-based sensors have some inherent drawbacks related to device stability, such as drift defined as a threshold voltage instability over time, characterised by a slow and unidirectional change of measured current or voltage and hysteresis appears as memory effect dependent of the history of samples (pH steps) experienced by the sensing electrode. The magnitude of these drawbacks may sometimes be larger than the requirements of some demanding applications. However, the overall low production cost beholds a great interest for some disposable-like applications, especially if the sensors are produced on disposable and eco-friendlier substrates such as paper.

2.2 Operating principle of FET-based sensors

A semiconductor has an associated net surface charge when in contact with an electrolyte solution mainly due to protonation and de-protonation, which has a direct impact on the effective gate voltage and hence on the charge carrier flow through the channel. This way, FET-based sensors have the ability to transduce biochemical binding events or ionic concentration changes on its sensitive surface into a measurable electrical signal based on the surface properties of the gate electrode [5]. Field effect transistors are devices with three terminals or electrodes – drain and source and gate, where the current flow between the first two can be modulated by varying the potential applied to the gate electrode. This generates a vertical electric field from gate to source whose intensity scales directly to the voltage applied to the gate [16]. Applying a positive or negative voltage at the gate can therefore increase or decrease the number of charge-carriers attracted to the channel, by accumulation or depletion, therefore switching the FET on or off. The current is conducted by one type of carriers (electrons or holes) depending on the semiconductor being n-type or p-type. In the later, the channel is in conduction when negative gate voltage is applied, needing positive voltages to repel the electrons from the semiconductor-insulator interface, generating a depletion layer free from electrons, that acts as an insulator (The opposite happens for n-type semiconductors). Thereby no current flows between source and drain, considering an infinite resistance between source and drain, which in reality is not the case, meaning that a small off current, normally in the range of picoampere (pA) will flow through the channel [5]. With this simple ability of tunning the channel resistance, the FET can be switched from what is conventionally called the OFF to the ON state. In the ON state the drain-to-source current (V_{DS}) varies with both the gate voltage and the drain voltage. Depending on the voltage applied across drain and source, a FET device has two regimes of operation: linear and saturation. The transfer characteristics of a FET device, allow the determination of electrical parameters that characterize these devices performance (e.g., threshold voltage; carriers mobility; ON/OFF current ratio) [4].

In the ISFET architecture, as stated, the insulator-gate mechanism, responsible for the operation of MOSFET, is replaced by an electrochemical gating effect [17]. In the most common form of ISFET, a dielectric insulator is present, and the capacitive coupling is dominated by the gate dielectrics. The most relevant parameter in ISFET-based sensors is the threshold voltage, as it is influenced by the flat-band voltage of the

gate/semiconductor/insulator capacitor structure. For a non-ideal device model, the flat-band voltage is different from zero, being its value reflected by the existence of oxide charges; the work function difference between the semiconductor and the solution; the reference electrode potential; the surface-dipole potential of the solution and the electrolyte/insulator interface potential; which is dependent on the ion concentration in the solution [18].

2.2.1 Oxide/Electrolyte interface & Sensing layer in ISFET

In ISFET, a constant and stable reference voltage is applied on the electrolyte solution through the external reference electrode. This voltage makes positive or negatively charged species, present in the solution to accumulate on the electrode's surface and the ion-sensitive layer, creating an electrical double layer (EDL) on the interface between the insulator and electrolyte, as shown in Figure 2.2 B. For example, if using an n-type semiconductor, positively charged ions from a given solution will be attracted to the semiconductor, right above the conduction channel between source and drain, which leads to an attraction of electrons to the channel [19]. If by the contrary, the solution is rich in negatively charged ions, at the interface between oxide and electrolyte, the charges will be opposite and therefore repel each other, which causes the channel conductivity to decrease. From this we can understand that the accumulation of the analyte at the top of the insulating layer can change the drain current [20]. The polarity of the EDL can be changed by switching the bias voltage in the solution, through the reference electrode and therefore varying the number of charge-carriers in the channel bringing the ISFET into the ON or OFF state (Figure 2.2 C and D). Apart from this, the accumulation of charges can also change the threshold voltage of the device.

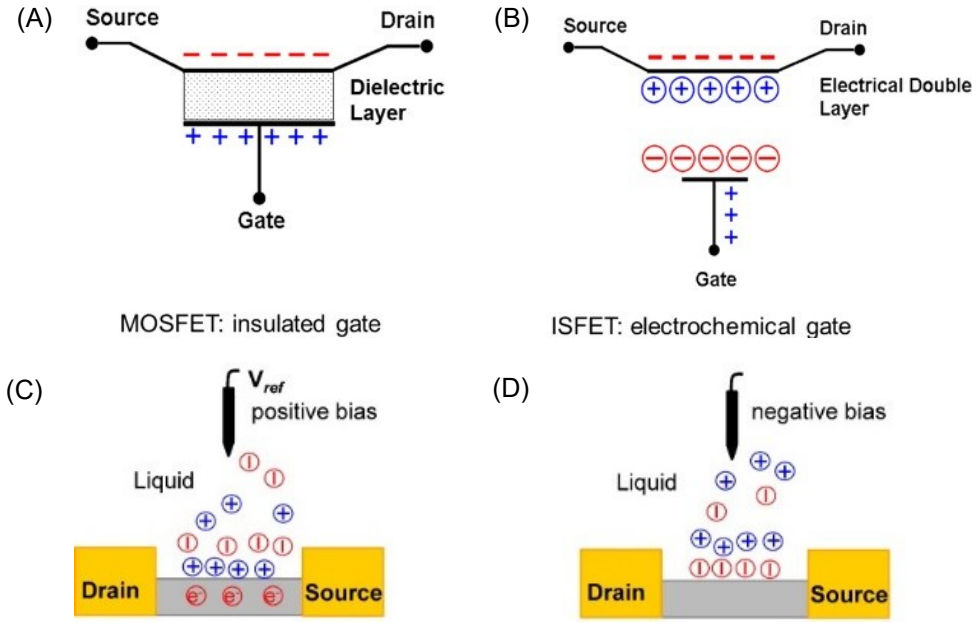

Figure 2.2 - Schematic representation of the operation principle of MOSFETs and ISFETs: (A) The three-electrode configuration in a MOSFET with a dielectric insulator material sandwiched between the channel and gate electrodes. (B) In the ISFET configuration the EDL forms at both electrolyte/reference electrode and electrolyte/oxide interfaces. (C and D) Applying positive and negative bias at the reference electrode changes the polarity of the electrical double layer. Requested with permission from [19].

The sensitivity of the sensor is therefore mostly dependent on the intrinsic properties of the sensitive layer and of the ionic concentration that is related to the Debye length. This parameter correlates the distance of the ions to the surface with its surface potential (Ψ). The closer the ions are to the sensitive layer, the greater the surface potential, reaching its maximum when ionic bonds are formed. An oxide's sensitivity can be characterized by

the parameter α. For a perfect sensitive oxide, α = 1. As so, theoretical maximum sensitivity can be calculated according to the following equations 1 and 2.

$$\alpha = \left(\frac{2{,}3k_B T C_{dif}}{q^2 \beta_{int}} + 1\right)^{-1} \quad (1)$$

$$\frac{\delta \Psi_0}{\delta pH_B} = -\frac{2.3k_B T}{q}\alpha \quad (2)$$

Where K_B is the Boltzmann constant, C_{dif} is the differential capacitance that represents the electrolyte's ability to adjust to the amount of charge due to a small change in the electrostatic potential. β_{int} is the oxide's intrinsic buffer capacity, which is related to the change in the total number of surface charge groups, which in turn is directly related to proton concentration variation.

Rearranging equation (2) the sensitivity is expressed as function of pH,

$$\Delta\Psi = \frac{2.3k_B T}{q}\Delta pH \quad (3)$$

This expression relates the surface potential variation due to a pH variation, and for an ideal sensitive oxide, a maximum theoretical sensitivity, known as Nernstian limit sensitivity, with a value of 59.2 mV/pH (at 25 °C) can be achieved [4].

2.3 Charge modulated field effect sensors

The typical ISFET device is obtained by substituting the transistor's gate contact with an electrolyte solution and a reference electrode. However, this design can lead to problems due to poor isolation between the device and the solution and it is also a blocking factor for miniaturization of ISFET devices. As such, research on this field has been made towards other ISFET architectures that would not need an external reference electrode or could incorporate one pseudo-electrode on chip or stacked in the device. An example of such accomplishment was the is the charge-modulated FET architecture (CMFET), introduced by Barbaro *et al* in 2006. This architecture is based on the floating-gate transistor which is then coupled with a control-gate that acts as reference electrode and a sensitive area activated by charge induction (Figure 2.3 A). Based on this concept Veigas *et al.* developed an innovative modular design comprising a flexible and disposable sensing electrode and a standard commercial MOSFET [21]. Since the transistor is activated acting on a control-gate capacitive-coupled to a floating gate, it is independent of the materials and overall intrinsic transistor characteristics. Having the sensor and the sensitive area separated from the transducer (MOSFET), which is encapsulated and integrated in the backend electronics. Thus, all post-processing steps of the sensitive area are kept away from the transducer and thus separate the wet from the dry area where the transistor is activated. Another benefit is having no contact between control gate and solution, which results in no need to use a reference counter-electrode [22,23]. This leads to incredible stability and lifetime, while lowering the overall complexity and production cost of the disposable sensing electrode. Figure 2.3 B shows the charge-modulated ion sensitive field-effect transistor (CMISFET) architecture. This structure resembles two capacitors in series connected via the extended gate.

The shown architecture works by the induction of charges at the interface of the extended gate electrode, bellow the sensitive area, through the chemical charges present in the solution that is in contact with the sensitive area. In Figure 2.4, the bound surface charge (Q_s) generates an electric field, inducing charge on the top side of the floating-gate, and since total charge in the buried gate must remain constant, an opposite charge appears on the bottom side.

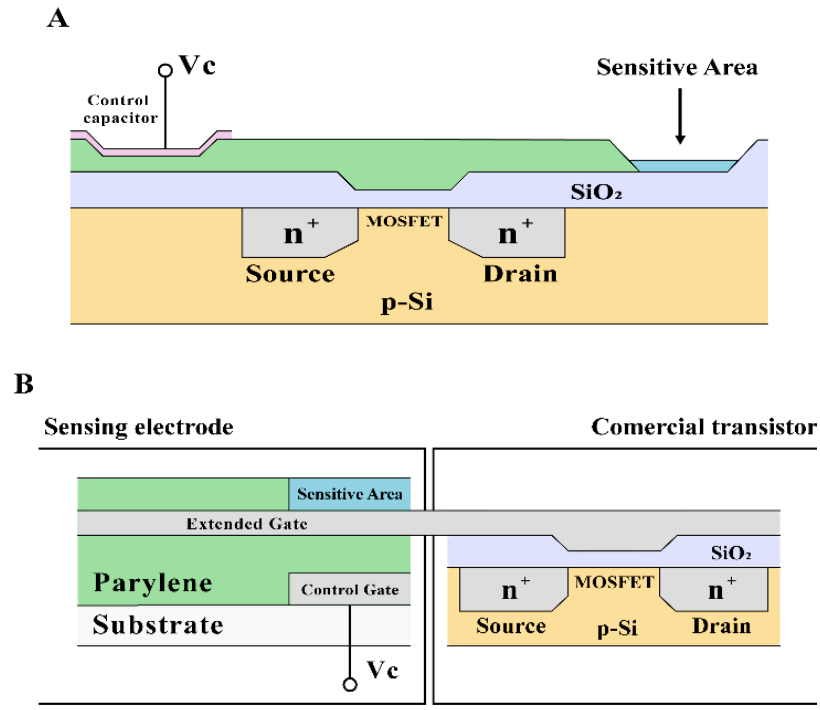

Figure 2.3 - Cross section schematics of CMFET architectures: (A) Integrated CMFET proposed in [22]. (B) Two-section CMISFET comprising a stacked control/sensing electrode and a standard commercial transistor. Adapted from [21].

As a result, charge carriers will be attracted or repelled (depending on silicon doping and charge sign) underneath the active area [24]. Thus, an electric field and, consequently, a voltage drop (V_{FG}) are generated between silicon substrate and extended gate. Therefore, the resulting voltage, has the ability to modulate the MOSFET's channel and give rise to its drain current. Of course, if the bulk is p-type and the surface bound charge is positive the native MOS transistor could be turned-on since the voltage drop would be positive; on the contrary, if the bound charge is negative the MOS transistor could not be turned on because of the negative sign of V_{FG}. The contrary is true in case of n-doped bulk. Moreover, through an applied bias voltage at the bottom electrode, the control-gate can be used to set the operating point of the device, zeroing the effect of unknown charge. For further details regarding the operation of this architecture, physical and mathematical modelling of the charge detection mechanism, readers may find a detailed explanation in [22].

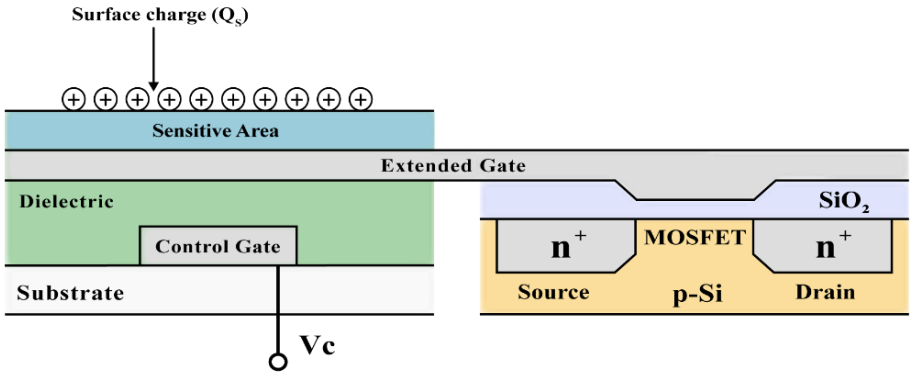

Figure 2.4 – Charge inducement on the CMISFET architecture through accumulation of ionic charges accumulating on top of the sensitive area. Adapted from [21].

CMFET architecture has shown to be able to detect charges and successfully detect DNA hybridization. The same device can be used for detection of any biomolecular process involving a change in electric charge [22], therefore being adequate to detect pollutants, such as metals and polycyclic aromatic hydrocarbons

(PAHs), which are present in marine environments and can increase oxidative DNA damage and prevent DNA repair [25]. It was not possible to identify CMISFET or ISFET devices with a comparable working principle in literature, however the results exhibited in Table 1 frame this architecture in relation to various other ISFET and extended gate FET sensing devices found in literature, some of them making use of identical materials and/or deposition techniques.

Table 1 – Comparison of various sensing films for FET sensors

Sensing film	Deposition technique	Sensitivity (mV/pH)	Ref.
SiO_2	LPCVD	27	[26]
SiO_2	PECVD	31	[27]
SiO_2	Thermal oxidation	30	[28]
SiO_2	Thermal oxidation	25	[29]
Si_3N_4	CVD	46	[30]
Si_3N_4	LPCVD	47	[31]
ZnO	RF sputteting	32	[32]
Ta_2O_5	RF sputtering	40	[33]
Ta_2O_5	Sputtering	56	[34]
Ta_2O_5	Sputtering and thermal oxidation	55	[35]
Ta_2O_5	RF sputtering and thermal oxidation	56	[36]

The technique used for depositing the sensing films on the substrates is also important for the overall sensing performance of an ISFET device. Each technique has its own advantages and limitations, and influence the films properties, such as strength and uniformity, that correlates to the pH sensitivity and sensing device performance [37]. Mainly chemical vapor deposition (CVD) and physical vapor deposition (PVD) techniques are used, and comparable sensitivities are achieved. CVD offers good quality and uniform films with controlled thickness but need high processing temperatures and precursors that may be toxic [38]. PVD methods such as radio frequency (rf) sputtering are a good alternative for the deposition of thin films for ISFET devices because they are compatible with a wide variety of materials delivering quality thin films and allow for room temperature deposition, which is compatible with low-cost, flexible and disposable substrates [4, 33]. CMISFET devices were produced in the scope of this project on flexible substrates such as PEN and cellulose based. The sensing film on these devices was deposited using rf sputtering and obtained sensitivity value on for devices on cellulose based substrates was 32 mV/pH which is on the lower side when compared to the various devices included in Table 1, however, the devices showed a remarkable stability over time with low drift and hysteresis.

3 Materials and methods

In this section, the procedure used to fabricate the sensors in all substrates is firstly reported. Following that, the electrical characterization protocol carried out for measuring the sensors response is described, as well as the protocol followed for data analysis.

3.1 Sensor fabrication

CMISFET sensing electrodes were produced in a stacked configuration on five different substrates: Corning glass; flexible and transparent polyethylene naphthalate (PEN); Whatman paper no. 1® with coating and CelSmartSense papers 15R, with and without an ethyl cellulose coating. The last two were developed in a previous project called CelSmartSense (LISBOA-01-0247-FEDER-017862). Each substrate was individualized in a 10 × 10 cm square where a total 5 × 10 sensors were produced.

Before sensor fabrication, both Whatman and CelSmartSense substrates were coated using a cellulose derivative: Ethyl cellulose (CAS: 9004-57-3 from Sigma Aldrich) in a mix solvent: 4-hydroxy-4-methyl-2-petanone ($C_6H_{12}O_2$, CAS: 123-42-2, 99 %, from Sigma Aldrich) and Ethanol absolute anhydrous (C_2H_5OH, CAS: 64-17-5 from Carlo Erba). As said, two different papers were used as substrates, Whatman paper no. 1 with minimum surface roughness of 11 μm and CelSmartSense, made of 100% pure eucalyptus fibres, with average roughness of 4.5 μm. On both Whatman and CelSmartSense papers with coating, the surface coating was applied using a doctor blade (Brand and Model). The coating solution consisted of 7.5 wt% ethyl cellulose (EC) which was prepared in a mix of 50DAA:50 Ethanol absolute. For each substrate, a total of 5 layers were deposited and left to air dry between each layer for around 30 min. A 4 μm calibration rod was used, with a speed of 2 m/min, at room temperature. For the PEN and corning glass substrates, an overnight thermal treatment was performed. The substrates were place in an oven at 150°C, and after this step were submitted to a cleansing process involving 10 minutes in ultrasonic bath of acetone, followed by 10 minutes of ultrasonic bath in isopropyl alcohol and rinsed with ultra-pure water. The majority of ultra-pure water was carefully removed with a nitrogen gun, and in a final step the substrates were placed in a hotplate for 20 minutes at a temperature of 120°C to make sure any left cleansing products were evaporated.

Regarding the sensor's fabrication, the layer's deposition sequence was molybdenum back control capacitor contact; parylene-C dielectric film (deposited in two sequential steps); molybdenum control capacitor top contact; Ta_2O_5 sensitive layer, as shown in Figure 3.1 A. Prior to each thin film deposition, each layer was patterned by aligning a physical mask, thus avoiding photolithography and lift-off techniques. For the deposition of 60 nm thick molybdenum thin films, a 3" target (3 mm thick, 99.95% purity; Alineason Materials Technology, Germany) was used with a deposition pressure of 0.23 Pa (1.7 mTorr), in an argon atmosphere (Ar = 50 sccm), and rf power of 175 W. Parylene-C (Speciality Coating systems, USA) was deposited in two subsequent depositions of 0.3 g, using silane as adhesion promoter, to obtain a ~400 nm dielectric layer. Standard deposition parameters were used: furnace temperature of 690 °C; pressure gauge temperature of 135 °C; vaporizer temperature of 175 °C on a Specialty Coating Systems Model PDS 2010 Labcoter™ 2. Since deposition pressure is directly related to the deposition rate and film quality, a compromise was found at 1.87 Pa (14 mTorr) slightly above the system base pressure of 0.8-1.07 Pa (6-8 mTorr). Tantalum oxide thin films were produced from a 3" (7.62 cm) Ta_2O_5 ceramic target (99.99% purity; Alineason Materials Technology, Germany) and deposited with a thickness of ~100 nm. Prior to deposition, pre-sputtering (sputtering with the shutter closed to prevent deposition) was performed for 10 min to ensure thin film reproducibility. The rf sputtering deposition parameters were previously optimized for higher pH sensitivity [4,37]. For this step,

deposition pressure of 0.3 Pa (2.3 mTorr), deposition gases ratio (Ar:O_2) of 14:0.5 sccm, and rf power of 150 W were used. A three-dimensional appearance of the CMISFET sensor is shown in Figure 3.1 B. For detailed information regarding the development and optimization of the production process, please read [21].

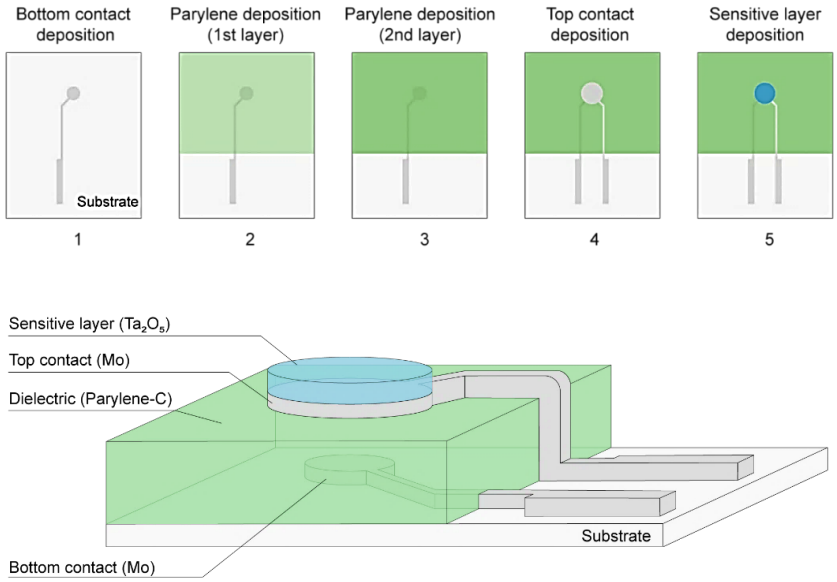

Figure 3.1 – CMISFET sensor fabrication: (A) Layer deposition sequence. (B) Device in a stacked configuration.

3.2 Measurement protocol

To perform the electrical characterisation of the sensors, an Agilent 4155 C semiconductor parameter analyser and Cascade Microtech M150 microprobe station was used altogether with Keysight EasyEXPERT group+ software. For this, an acrylic cell with a ZIF socket (with exception for the sensors produced on corning glass) was integrated into the probe station with the sensors being inserted in the later at fixed a parallel position and connected through the ends of the socket to a breadboard which was used to facilitate all connections between the sensor, MOSFET (CD4007UB) and the probe station SMU ports. Experimental setup is shown Appendix A.3. CMISFET sensors were evaluated using two different testing methodologies: i) measuring the transfer characteristics curves, with the MOSFET operating in the saturation regime with (V_{DS} = 0.5 V) and V_G swept between 0.8 V and 2 V. the hold and delay times were fixed at 1 s and voltage steps of 100 mV (measurement speed of 100 mV/s). The reference drain current (I_D) was obtained at V_G = 1.7 V and plotted against pH to extract the sensitivity in µA/pH. The sensitivity in mV/pH was also extracted from the transfer curves by doing a linear regression at the region of transfer curves where the data showed to be linear ($V_{GS} >> V_{th}$). V_G values at a fixed drain current between 200-300 µA where then respectively plotted against each pH buffer solution. ii) performing real time monitoring of the drain current. For these measurements, constant gate (V_G = 1.7 V) and drain voltages (V_D = 0.5 V) were applied with a compliance current of 100 mA. The drain current is acquired with sampling intervals of 1 second.

3.2.1 CMISFET sensor testing

Sensors were tested at room temperature (T ≈ 25°C). When starting to evaluate a sensor a first dry test was performed. Three to five consecutive measurements were performed without any buffer solution added, spaced within an interval of three minutes, to check if the signal added to the bottom electrode is transferred to the MOSFET gate, if so, typical exponential transfer curves were obtained. Only after this preliminary test, the sensors were measured through.

For each method described, the sensors were tested using pH buffer solutions of 4, 7 and 10 with precision of ± 0.01 (HANNA instruments). First, 6 μL of pH 10 buffer solution are pipetted onto the sensitive area of a sensor. The solution was maintained for 10 to 30 minutes for the sensing platform to stabilize, while monitoring the output response as stabilization time is not linear. This was performed for sensors on all before starting a measurement cycle. When performing the voltage sweeps to extract the transfer characteristics, a first measurement of I_{DS} vs V_G is performed and after that several measurements spaced in time (~3 min) are taken until there is no significant shift (≤ 0.5 μA). The last measurement will therefore represent the pH 10 reference measurement, and I_{DS} reference value for that buffer solution. After this an exchange in pH solution was performed (from pH 10 to pH 7). With the micropipette the previous solution was removed, without the need to clean the surface or to try to remove all the pH buffer solution. Instead, the new solution was added with the micropipette (using a different tip) so that the surface of the sensor is always wet. The new solution was added, and removed, added a new volume, removed again, and added for a final time, to assure the solution placed onto the sensitive area is completely renewed with no previous solution left. After stabilization, the final curve acquired represents the reference pH 7 I_{DS} curve. Finally, an exchange of solution to pH 4 was performed and the data was collected with the same procedure as stated above. Two more cycles of pH10 → pH7 → pH4 were performed, for a total of 3 cycles to have a statistically significant variability and knowledge of the sensor's stability. A similar procedure was used for the continuous real time monitoring of the drain current. Like in the previous method, a first pH solution (6 μL) was pipetted onto the sensitive area and left to stabilize for 10 to 30 minutes. After stabilization, a first measurement cycle was performed. In this method of analysis, an additional reverse measuring step of buffer solutions was introduced, thus having a full cycle of pH samples in contact with the sensing electrode (10 → 7 → 4 → 7 → 10), which was again repeated two times, for a total of three measurement cycles. During continuous real time monitoring, each pH buffer solution was left to stabilize until sufficient data points (~300 s) showed no significant variation.

3.2.2 Data analysis protocol

To analyse and discuss the data recorded from the transfer characteristics and continuous real time measurements, an analysis algorithm was constructed. Firstly, the bulk data from all sensors from each batch was analysed considering the two measurement methodologies, thus having transference characteristics plots and real time measurements plots. From the first methodology, the sensitivity in μA/pH and mV/pH was extracted, while from the real time plots only the sensitivity in μA/pH could be extracted. After having all sensitivities from each cycle and an average for each sensor, the average sensitivity and corresponding error for the sensors on a given substrate were recorded.

However, it was noted that sensors from each batch were showing considerable variation in the current levels for each pH, resulting in averages that contained a relatively high error associated. Since the differences between current levels for the pH solutions used was more or less consistent in all sensors, two normalization methods were conducted. In method 1, to a given level of current associated with a pH solution, a reference current (I_0) was subtracted. In this case pH 10 associated drain current was considered as I_0, returning absolute error like values for each pH associated drain current, $\Delta I_D = I_{Dx} - I_0$. The second method of normalization was a relative weighting of the results, which took the results from the first method and divided them by I_0, having, $(I_{Dx} - I_0)/ I_0$. Both approaches showed to be effective reducing the overall error associated with the spread of data. Signal to error ratio was used as a coefficient to compare both methods, from which both methods exhibited identical ratios. This way, the first method was the chosen one to show in this work, since it is clear to understand and interpret the results.

4 Results and discussion

In this chapter, an analysis of the obtained results for CMISFET sensors produced on all substrates is presented. The chapter starts with a comparison between two connection topologies of the CMISFET sensors. This comparison is established between sensors on PEN substrate, which were already used in previous projects at CENIMAT, and new sensors developed for the first time on cellulose-based substrates in collaboration with AlmaScience. This is an eco-friendlier and lower cost approach for this sensing architecture. Afterwards, the optimization of the detection protocol for the maximization of signal resolution and signal to error ratio is explained and again justified for the sensors on PEN and paper substrates. Next, the sensors produced on cellulose-based substrates are analysed in accordance with the optimal sensor connection topology, where all results shown were compiled following the data analysis protocol defined in Chapter 3. Sensors produced on different paper substrates are compared mainly through their sensitivities from different measurement methodologies and standard deviations, which were considered as error, throughout the discussion of results. In the end a final comparison of the performance of sensors on cellulose-based substrates versus the sensors produced on reference substrates – PEN and corning glass, is performed. Sensors produced on corning glass substrate were used as the reference, since corning glass is an inert, rigid and has a smooth surface, preventing deformation-based degradation during sensor production, handling and measurement protocols.

4.1 Optimization of the detection protocol

It is known that the detection protocol is directly related to the results obtained in terms of signal and error. For this matter, a comprehensive study was conducted on sensors fabricated on PEN and cellulose-based substrates in order to attain an optimal detection and data analysis protocol to compare the results of sensors produced on different substrates.

4.1.1 CMISFET sensor connection topology

CMISFET sensors were tested with a different connection topology, other than the standard one showed in Figure 4.1 A. where the control voltage is applied in the bottom electrode, previously reported in [6]. The contacts were inverted, thus applying a bias voltage in the top electrode and connecting the MOSFET gate to the bottom electrode, as shown in Figure 4.1 B. For the sake of simplicity, the “standard” connection topology is considered as connection topology A and the “inverted” connection topology is considered as connection topology B. Thus, the measurement protocol was carried out to test both connection topologies. pH monitoring was performed with the following sequence: pH 10 → pH 7 → pH 4 for the transfer characteristics extraction and pH 10 → pH 7 → pH 4 → pH7 → pH10 for the real time continuous monitoring. First, the transfer characteristics where extracted. Figure 4.2 shows a side-by-side comparison of the results of one sensor using both connection topologies. In the transfer curves it is firstly noted that the V_{th} due to the pH solutions applied shift in opposite directions, represented by the blue arrow in both figures. This phenomenon is related to the induction that happens when charges (Q_S) accumulate at the surface of the sensitive layer. For topology A, induction of charges occurs directly in the top contact thus, the increase in proton concentration (lower pH) leads to a variation of the Ta_2O_5 sensitive layer surface potential and consequently to the increase of channel current (I_D). This was observed considering the transfer curves obtained with V_D = 0.5 V, where the channel current increased when changing from pH 10 to pH 7 and subsequently to pH 4, indicated by the blue arrow in Figure 4.2 A. When using connection topology B, the inverse happens, since induction of charges that modulate the MOSFET channel happens at the bottom electrode. Here, the charge in the bottom electrode is a

result of the sum of charge resultant by the induction at the top electrode and those injected by the reference voltage.

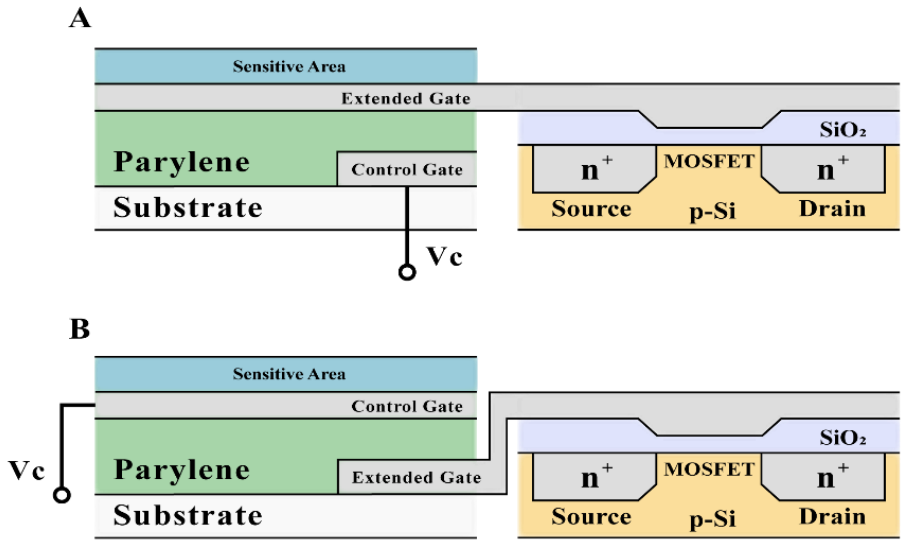

Figure 4.1 - Connection schematic of CMISFET sensor: (A) standard connection topology, having the top extended gate electrode connected to the MOSFET and inducing charges through the voltage (V_C) applied on the control gate. (B) Proposed connection topology having the bottom electrode control gate connected to the MOSFET and applying voltage (V_C) on the top extended gate electrode. Adapted from [21].

When comparing the results of both connection topologies, it is notorious that topology B shows a greater separation between pH levels, confirmed by the extracted sensitivities. Figure 4.3 A and B show this metric in mV/pH which is the most common approach to evaluate the device performance found in literature, while Figure 4.3 C and D show the sensitivity in µA/pH. This last representation is also approach and can be directly compared with the one obtained from the continuous real time monitoring. The values of V_G at a fixed current (I_D = 300 µA), and of I_D at a fixed control voltage, V_C = 1.7 V, associated to all three pH solutions tested are plotted against pH and linear fits are performed, from which the slopes return the corresponding sensitivities.

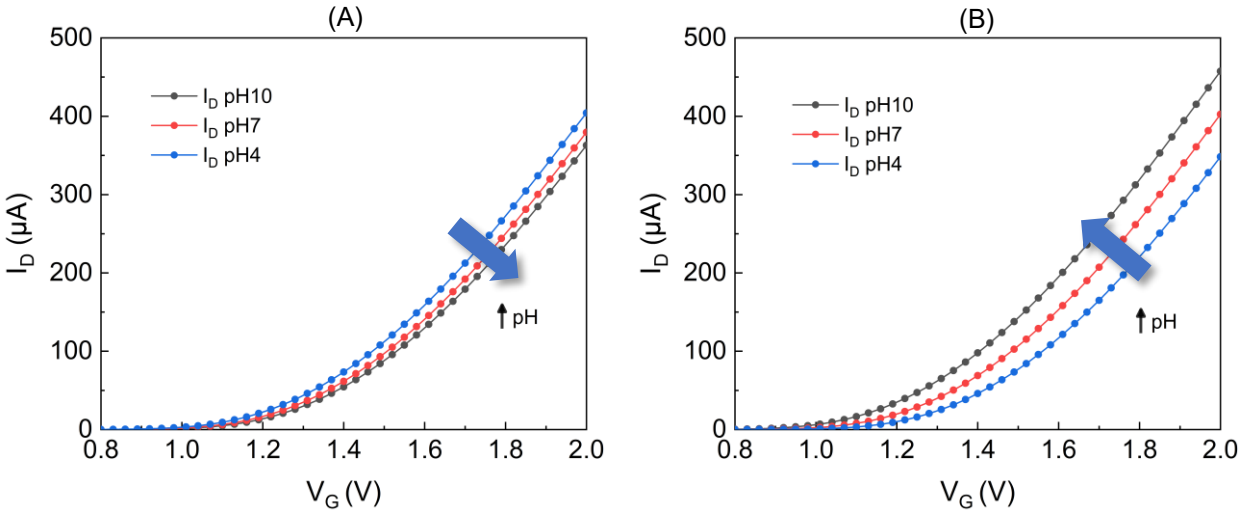

Figure 4.2 – pH sensing performance of a tested sensor on PEN substrate, evaluated through transfer characteristics with V_D = 0.5 V: (A) Transfer characteristics obtained for the standard connection topology. (B) Transfer characteristics obtained for the inverted connection topology.

From three tested sensors, connection topology A showed average sensitivities of 9.5 ± 1.5 mV/pH and 4.87 ± 0.7 µA/pH, having a maximum sensitivity of 11 mV/pH. These values which are in agreement with previous results obtained of 12.0 ± 2.0 mV/pH using this architecture [23]. On the other hand, using connection topology B, greater sensitivities of 27.7 ± 2.0 mV/pH and 14.0 ± 0.2 µA/pH were obtained. This represents an increase in sensitivity of almost 200%, while maintaining equal or inferior associated error. Moreover, when comparing the sensitivity linearity shown by both connection topologies (Figure 4.3), standard connection results showed a higher sensitivity for the pH range between 4 and 7 comparing to the range from 7 to 10. This in fact occurs naturally due to an effect known as the point of zero charge (pH_{pzc}) of the sensitive material, being higher for solutions with pH within two units of the pH_{pzc} of the sensitive material which for Ta_2O_5 is within the range $4 < pH_{pz} < 5$ [4,37]. However, by using the inverted connection topology, results show that the sensitivity obtained tends to be more homogeneous in terms of linearity for the whole range of pH. Although this was not a staple for all tested sensors, the majority showed a linear sensitivity throughout the range of pH, shown by the R^2 coefficient, which was always greater for the inverted connection topology. This is preferred as the sensor outputs a more predictable behaviour.

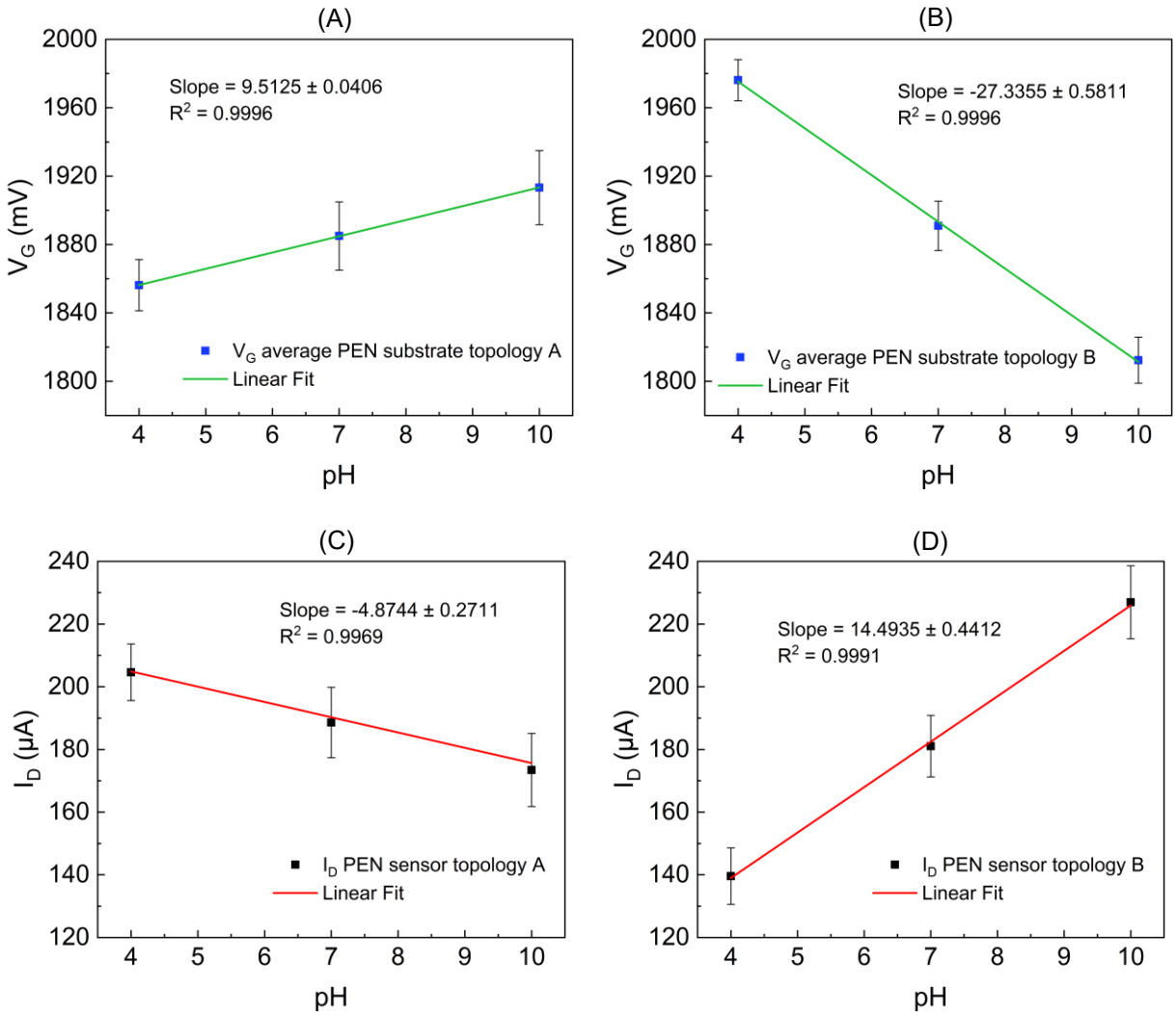

Figure 4.3 – Sensitivity extracted from the transfer characteristics shown in Figure 4.2. (A and B) sensitivities in mV/pH and (C and D) sensitivities in µA/pH extracted from the transfer characteristics of sensors connected in a standard connection topology and inverted connection topology, respectively.

Following this measurement, continuous real time tests were conducted. Figure 4.4 shows a side-by-side comparison of the obtained results from one measurement cycle, when using both connection topologies.

In a first analysis it is possible to see the behaviour depicted in Figure 4.4 A, shows more noise than Figure 4.4 B.

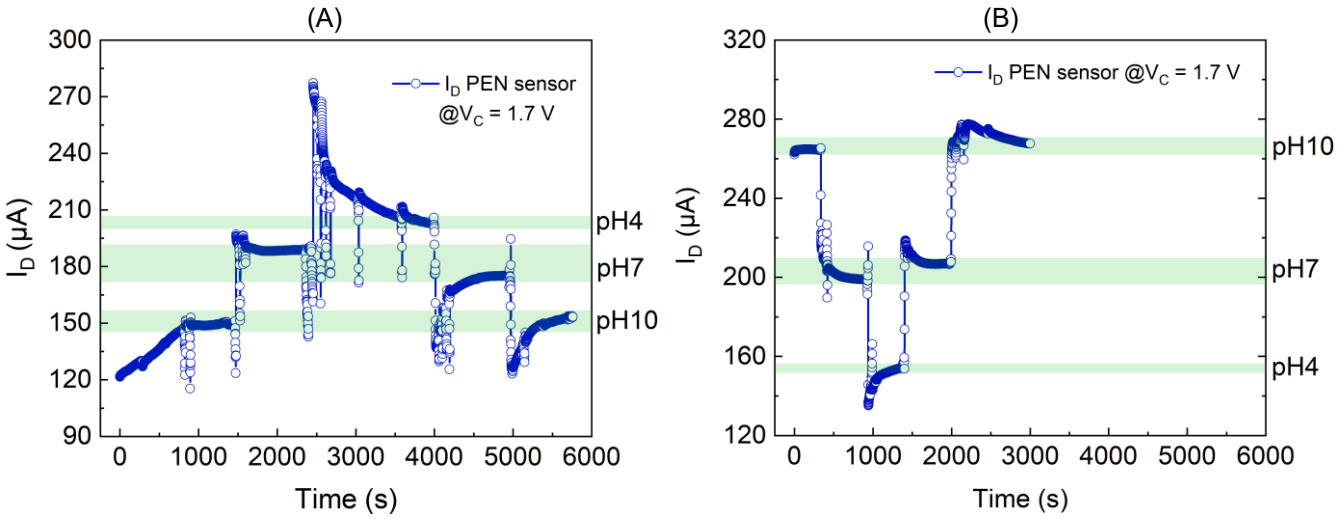

Figure 4.4 – CMISFET with sensing electrode on PEN substrate - pH sensing performance evaluated through continuous real time response of the drain current I_D at a fixed control voltage of V_C = 1.7 V: (A) Real time behaviour obtained for the standard connection topology. (B) Real time behaviour obtained for the inverted connection topology.

Hysteresis is also noted and despite being present when using each one of the connection topologies. Topology A has shown a higher tendency regarding this phenomenon, especially when looking at the transitions pH7 → pH4 and pH4 → pH7 in one cycle. Again, this is influenced by the pH_{pzc} of the sensitive oxide, that tends to be more relevant when using the standard connection topology. Considering the three tested sensors, continuous real time monitoring also showed much lower average sensitivity for the connection topology A, with higher associated error (4.9 ± 2.5 µA/pH), as with connection topology B, an average sensitivity of 16.9 ± 0.3 µA/pH was obtained. Moreover, the stabilizations time was faster, which resulted in a decrease in almost half of the real time monitoring full cycles when using the connection topology B, which is always preferable in a practical context (Figure 4.5).

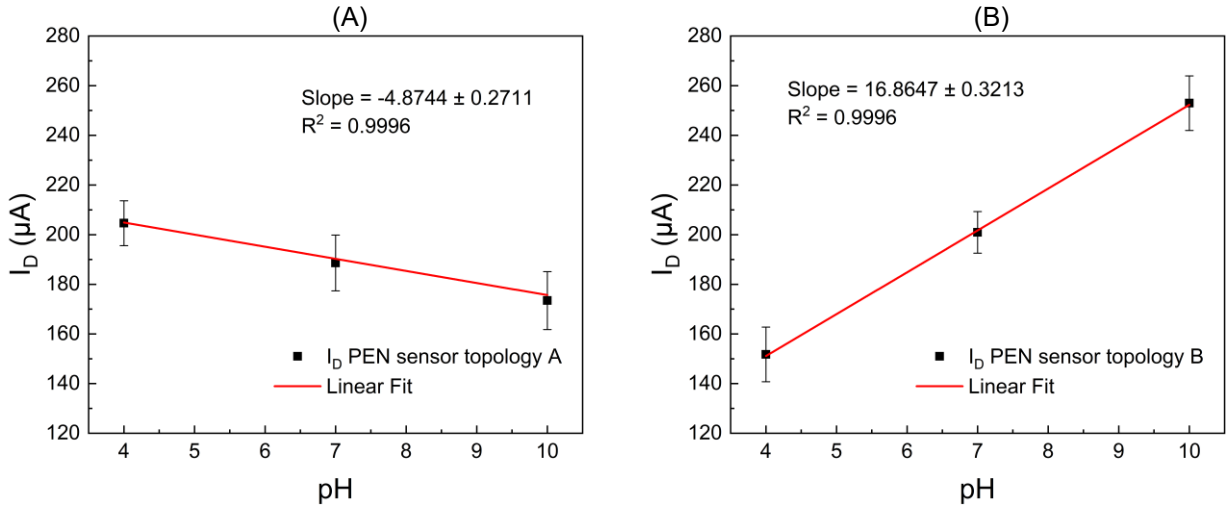

Figure 4.5 – Sensitivities in µA/pH extracted from one sensor on PEN substrate measured through real time monitoring curves shown in Figure 4.4. (A) sensitivity of sensor connected in a standard connection topology. (B) sensitivity of sensor connected in an inverted connection topology.

Following these results, sensors fabricated on CelSmartSense paper were also tested using both connection topologies, in order to see if the tendency obtained for sensors on PEN substrate was followed to the

cellulose-based counterparts. The transfer characteristics extracted using each connection topology are shown in. Figure 4.6 A and B. Three working sensors were tested and similarly, to the previous obtained results for sensors on PEN substrate, the sensors on CelSmartSense paper showed an average sensitivity of 8.0 ± 1.6 mV/pH using connection topology A and 31.7 ± 6.2 mV/pH using connection topology B. This represents yet again another rise in sensitivity of 300%.

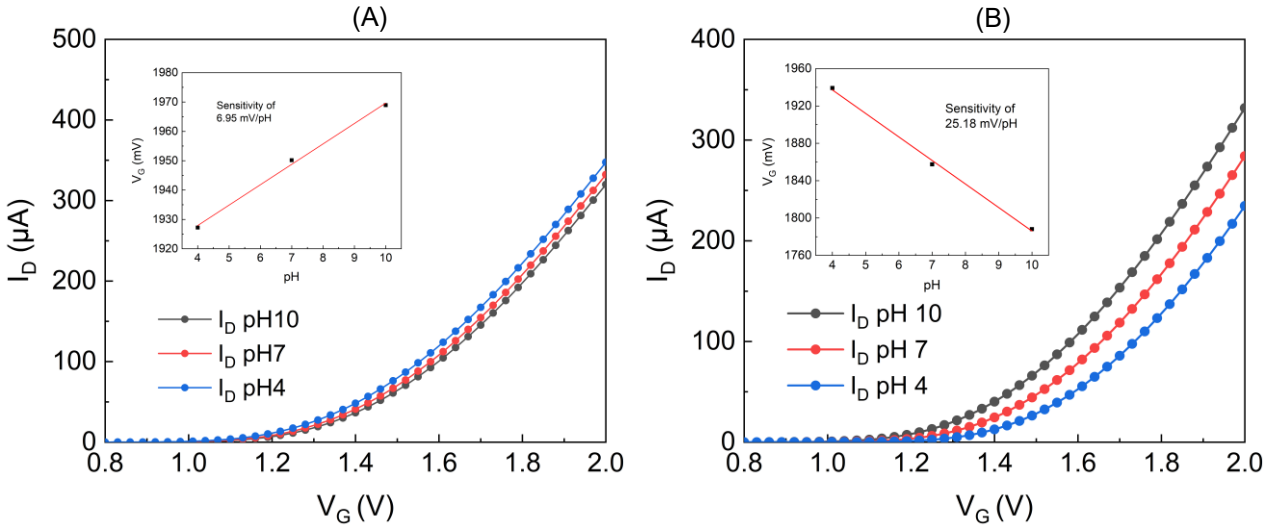

Figure 4.6 - pH sensing performance of a tested sensor on CelSmartSense with coating substrate evaluated through transfer characteristics with V_D = 0.5 V: (A) Transfer characteristics obtained for the standard connection scheme. (B) Transfer characteristics obtained for the inversed connection scheme.

Sensitivity results in µA/pH were also extracted from the transfer characteristics. For connection topology A, a sensitivity of 4.3 ± 0.7 µA/pH compared to 14.2 ± 0.2 µA/pH obtained with connection topology B. Following this, real time monitoring of the drain current (I_{DS}) at a constant control voltage V_C = 1.7 V was performed (Figure 4.7 A and B). Likewise, the signal looks less noisy when using connection topology B and hysteresis is noted again for results obtained using connection topology A, especially on the pH7 and pH10 associated drain current levels from the direct and reverse order of testing. Sensitivity shows again to rise, in this case from an average of 6.7 ± 0.8 µA/pH to 17.7 ± 0.4 µA/pH, which represents a rise of approximately 170% in sensitivity, while keeping an identical associated error.

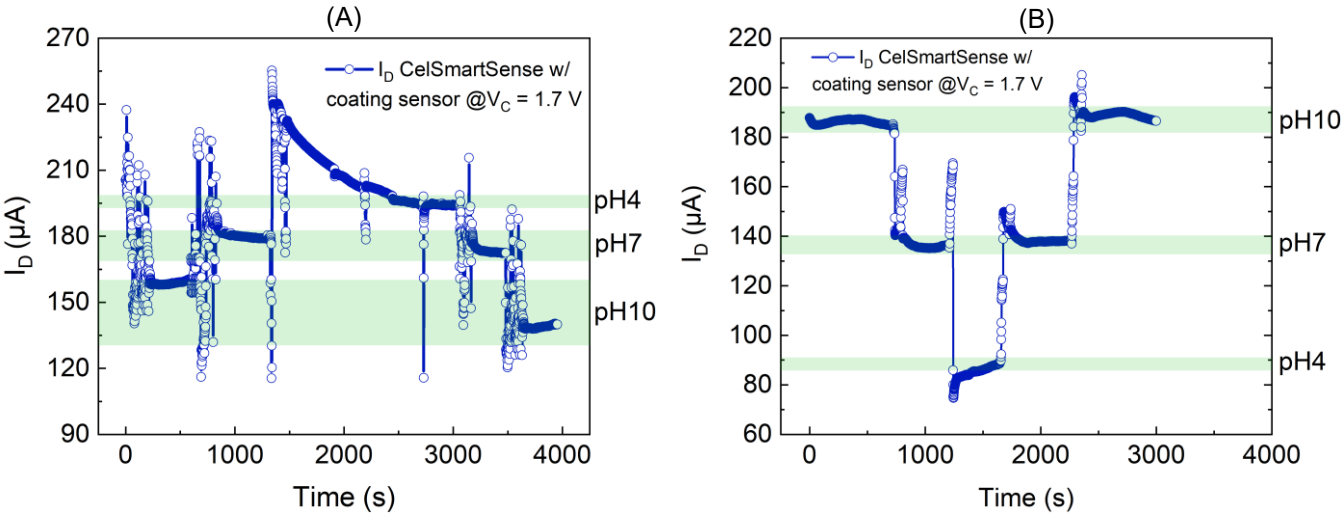

Figure 4.7 - CMISFET with sensing electrode on CelSmartSense with coating substrate - pH sensing performance evaluated through continuous real time response of the drain current I_D at a fixed control voltage of V_C = 1.7 V: (A) Real time behaviour obtained for the standard connection topology. (B) Real time behaviour obtained for the inverted connection topology.

A summary of the obtained results for this direct comparison is shown in Table 2. As seen, when connecting the sensor following connection topology B, an average enhancement in sensitivity of 200-300% is noted in both measurement methodologies on the tested substrates, while keeping an identical signal to error ratio. Real time monitoring results are overall less prone to noise, and stabilization of the drain current for each pH buffer solution was about 1.7 times faster when using connection topology B over connection topology A. Moreover, results obtained with the inverted connection topology tended to be more linear throughout the tested pH range, as shown by the R^2 coefficient of the linear fits performed. Here, having V_C applied right under the sensitive area affects the electrophoretic mechanism of charge induction. The approximation of ionic charges to the sensitive surface seems to be no longer ruled by the pKa of the oxide material, but instead forced by the superimposed potential applied underneath the sensitive layer. Side by side results of the real time monitoring using both connecting topologies prove a clear enhancement of the charge inducing process, since the average duration of a full measurement cycle is reduced by half. This can represent a huge advantage for the sensing of other analytes such as bigger molecules (e.g. biomolecules), to facilitate attraction to the sensitive area surface. However, more practical tests need to be conducted to sustain accurate conclusions on the electrochemical phenomenon behind this effect.

Table 2 - Sensitivity results obtained for sensors on PEN and paper substrates when using connection topology A and B.

	Connection topology A			**Connection topology B**		
	Sensitivity [mV/pH]	Sensitivity [μA/pH] [1]	Sensitivity [μA/pH] [2]	Sensitivity [mV/pH]	Sensitivity [μA/pH] [1]	Sensitivity [μA/pH] [2]
PEN	9.5 ± 1.5	4.9 ± 0.7	4.9 ± 2.5	27.7 ± 2.0	14.5 ± 0.2	16.9 ± 1.0
CelSmartSense w/ coating	8.0 ± 1.5	4.3 ± 0.7	6.7 ± 0.8	31.7 ± 6.3	15.5 ± 3.4	17.8 ± 0.4

[1] Sensitivity extracted from transfer characteristics; [2] Sensitivity extracted from real time monitoring.

In line with the obtained results, the rest of this chapter will focus on the results of sensors in different substrates, tested following this optimized detection protocol, where the topology of detection is connection topology B.

4.1.2 Signal extraction methodology: transfer sweep versus real time analysis

To infer about the optimal sensor testing methodology for extraction of the sensitivity, results obtained when extracting the sensitivity from the transfer characteristics are compared to the ones obtained from the real time analysis, again for sensors fabricated on PEN and CelSmartSense substrates.

An example of the obtained transfer characteristics are shown for a sensor on PEN substrate in Figure 4.8 A and for a sensor on a cellulose-based substrate with coating in Figure 4.8 C, which were extracted for each different pH solution after stabilization. From these curves, the sensitivity in mV/pH was extracted. In this case 27.7 mV/pH was the obtained sensitivity for that given cycle for the sensor on PEN and 30.1 mV/pH for the sensor on CelSmartSense paper - noting that this value is extracted from the V_G values at a chosen drain current I_D which intersected all reference curves in a linear region, far from the non-linear region at the knee of the curves (for the majority of the sensors this value was around 300 μA). Secondly, real time continuous

monitoring of complete cycles was performed, shown in Figure 4.8 B and D again for PEN and CelSmartSense substrates, respectively. Here, only the stabilization region was considered for the averages performed on each pH reference drain current. This method was preferred to have a clearer notion of the shifting of drain current through time, and also infer on the hysteresis of the sensors. A tendency to this unideal behaviour was especially noticeable for both sensors in the step differentiation between pH7 → pH4 → pH7 and sometimes also in the pH10 drain current levels. When reversing the order, the stabilization of drain current induced by the pH7 buffer solution happened in values either lower or higher than the first pH7 stabilization. This is related with a memory effect known as hysteresis that arises from the continuous accumulation of H^+ ionic charges from the tested solutions in the oxide sensitive area interface, which causes degradation the induction mechanism, shifting the effective threshold voltage of the MOSFET. Nevertheless, this effect resulted in shifts of current inferior to 10 µA for sensors on PEN and CelSmartSense substrates, which is not of great impact on the ability of the sensing device to distinguish the tested solutions.

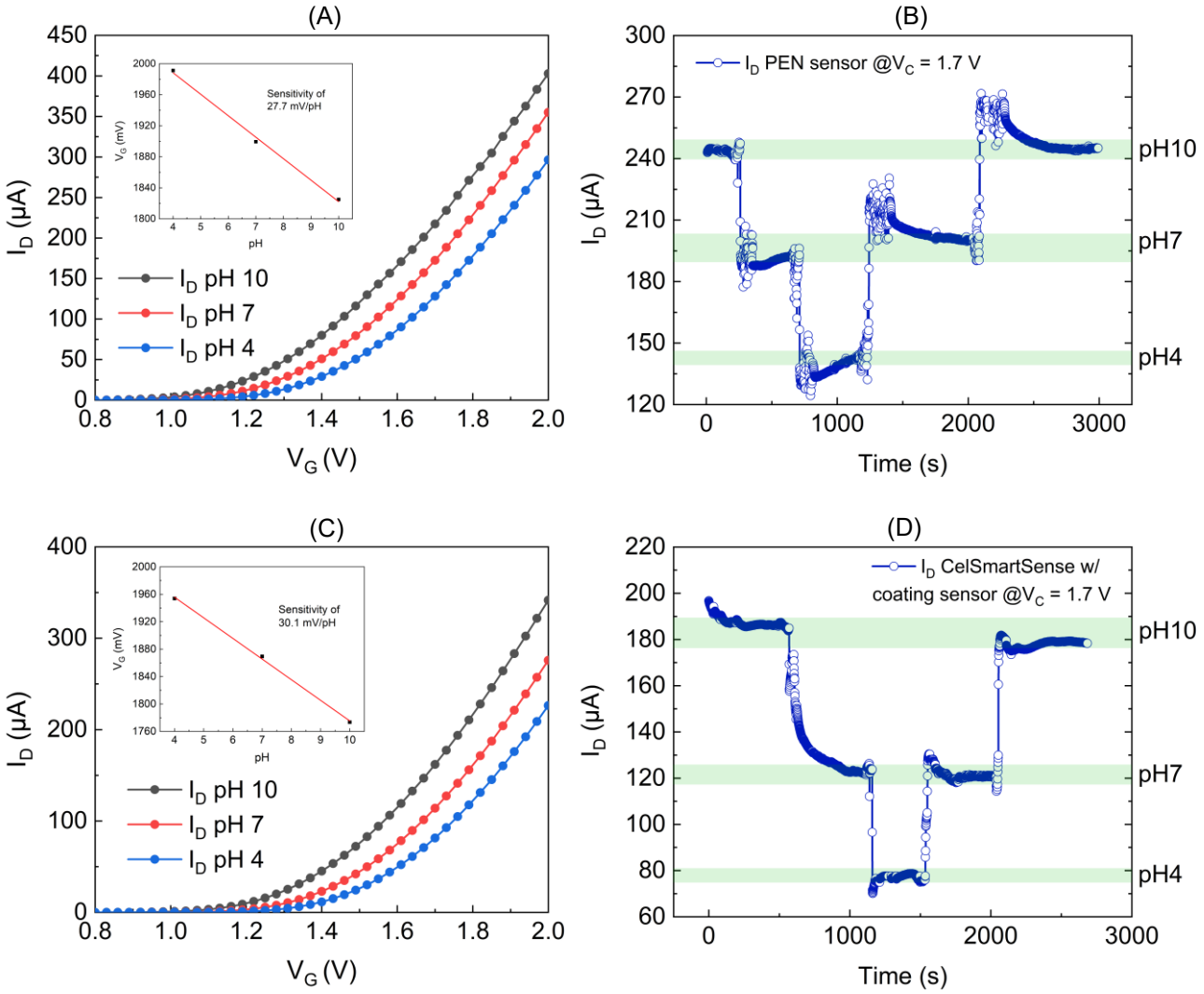

Figure 4.8 - CMISFET pH sensing performance methodologies for two individual devices: (A and C) Transfer characteristics obtained at a constant V_D = 0.5 V for a complete pH cycle, with curves expressed as variation of the reference drain current I_{DS} at a fixed gate voltage V_G, for sensors on PEN and CelSmartSense w/ coating substrate, respectively; (B and D) Continuous real time monitoring of the drain current I_{DS} at a control voltage of V_C = 1.7 V for a complete cycle of pH measurements for sensors on PEN and CelSmartSense w/ coating substrate, respectively.

Three working sensors of the same batch were tested for pH sensitivity under the defined protocol. Graphical representation of the normalized I_D variation with sample pH (ΔI_D pHx-pH10) allowed to compare pH sensitivity for all the sensors on one specific substrate and later compare sensitivity values for sensors on

all tested substrates. The only downside of this comparative analysis method is the loss of information regarding the error associated to pH 10 measurements, given that I_D pH10 is the reference. However, it was noted that pH 10 buffer solution was in fact the one that produced the smaller sensing deviation in current, for sensors of the same batch. This may be due to the fact of having the pH10 solution as the first to be in contact with the sensing electrode in each new cycle, and this way hysteresis was minimal in between cycles. For the first sensor on PEN substrate tested, the results from transfer characteristics cycles and real time continuous monitoring cycles are shown in Figure 4.9 A and B, respectively. Sensors on CelSmartSense substrate showed an identical behavior. Graphical representations are shown ahead in subchapter 4.2.

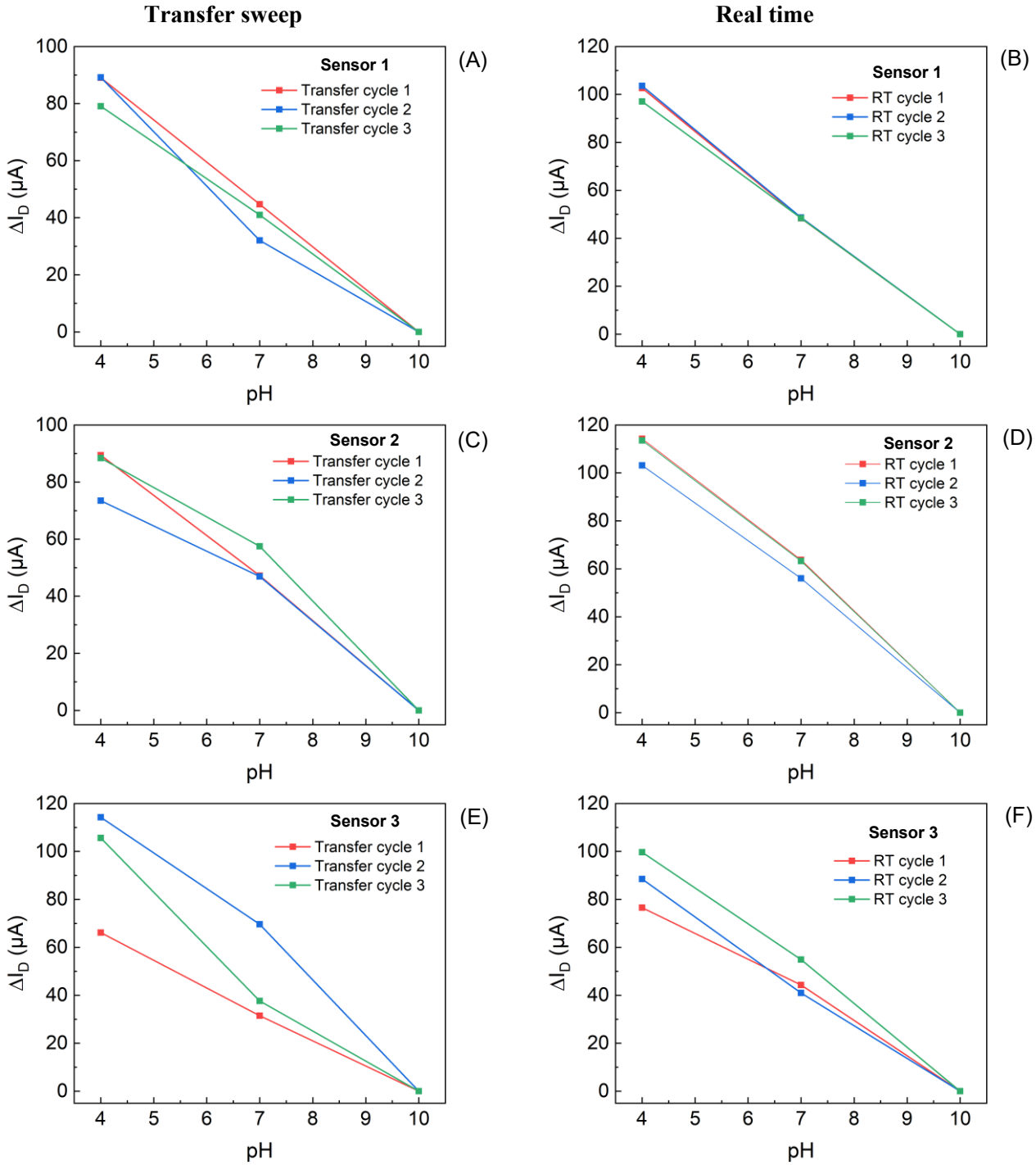

Figure 4.9 - Sensitivity analysis of three tested sensors on PEN substrate. (A and B); (C and D); (E and F) results extracted from transfer characteristics and real time continuous monitoring, respectively, for the three tested sensors. Noting that the connecting lines between the dots is only to facilitate the reading of the slope tendency and does not represent any data values.

In a first comparison between transfer characteristics and real time monitoring, the precision of the later in terms of sensitivity is higher in between cycles, also given to the fact that there is less variation for pH's 4 and 7 associated measurements over cycles. In practice, the obtained signal to error ratio, being error considered as the standard deviation between ΔI_D (pHx-pH10) in between cycles, was about three times higher for the real time monitoring in relation with the transfer characteristics. Such greater variation happening in the transfer characteristics extraction method may originate from some factors – one being that when performing the transfer characteristics, each time an IV curve was acquired, stress is induced in the MOSFET, which over time may lead to some inherent variation; another factor is that through real time monitoring it was possible to have a much clearer notion of the drift tendency and consequently when stabilization happened. Another possibility ties with the fact that real time monitoring of the drain current being performed after the extraction of the transfer characteristics, which may have served as a complementary preconditioning and contributed to a further activation of the sensitive area of the sensor. This is unlikely, however, it is possible to infer through an analysis of the sensitivity variation over cycles for sensors tested on both PEN and CelSmartSense substrates, depicted in Figure 4.10 A and B, for the first ones, and C and D for the second, for both transfer characteristics and real time monitoring cycles, respectively. By looking at the transfer cycles and focusing on each sensor individually, a clear tendency for the sensitivity over the cycles did not exist, so there is no evidence of a direct influence of preconditioning. However, it is notorious that the sensitivity deviations are greater when extracted from the transfer characteristics both intra and inter sensor measurement cycles. This is most likely tied with the induced stress in the MOSFET, which through the cycles caused some inevitable variation in the transduced current I_D, resulting in a degradation of the signal to error ratio.

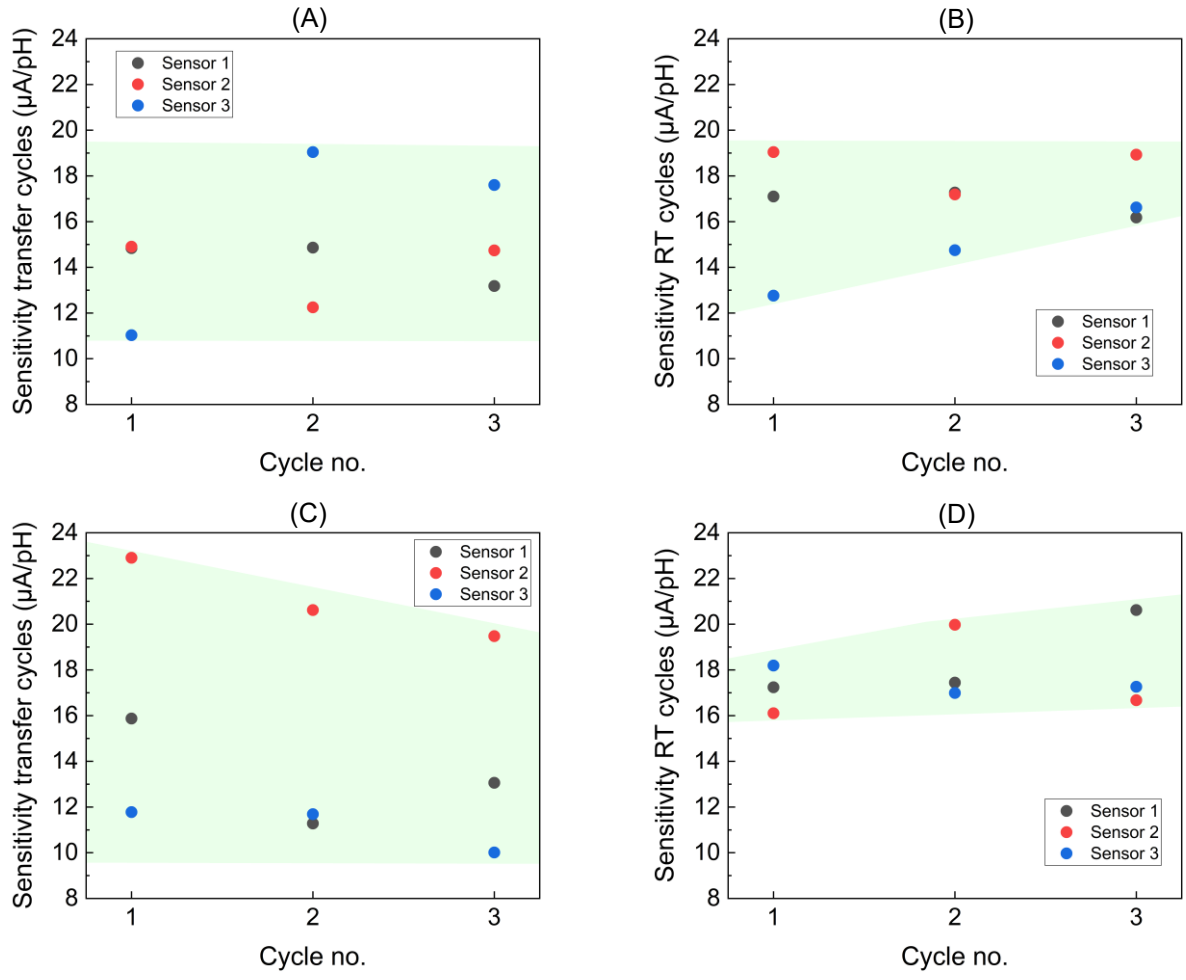

Figure 4.10 - Sensitivity variation throughout testing cycles of sensors on PEN and CelSmartSense with coating substrates. (A and C) Transfer characteristics cycles. (B and D) Real time monitoring cycles, respectfully in order for each substrate mentioned.

In order to obtain the sensitivity for each sensor, data from all sensors cycles was compiled, returning the averages extracted through each measurement method, which are shown in the following Figure 4.11 A, B and C. Graphical results of sensitivity obtained using both signal extraction methodologies for sensors on CelSmartSense paper substrate, are in line with the ones shown for PEN and can be found in the next subchapter 4.2. The sensitivities obtained were higher for the real time monitoring measurements, in the first and second sensors tested, while also maintaining smaller error in between cycles. Only the third sensor showed a different behaviour, exhibiting very close sensitivities for both the data extracted through transfer characteristics and real time monitoring, but again showed a clear tendency for greater error associated to each pH. By looking into Figure 4.9 E, which refers to the transfer characteristics measurements on PEN sensor three, here the absolute difference ΔI_D (pH4-pH10) obtained for the pH 4 data point was considerably lower than the other two, but still inside an acceptable range. With this in account and having in mind the preconditioning the sensors were exposed to before measurements, the cycle was still considered for the effective average of the sensor's sensitivity through transfer characteristics extraction.

The obtained results for each sensor are outlined in Table 3. The results in mV/pH were directly obtained from the transference characteristics at a given reference current and both sensitivities in µA/pH were extracted from the analysis protocol carried out.

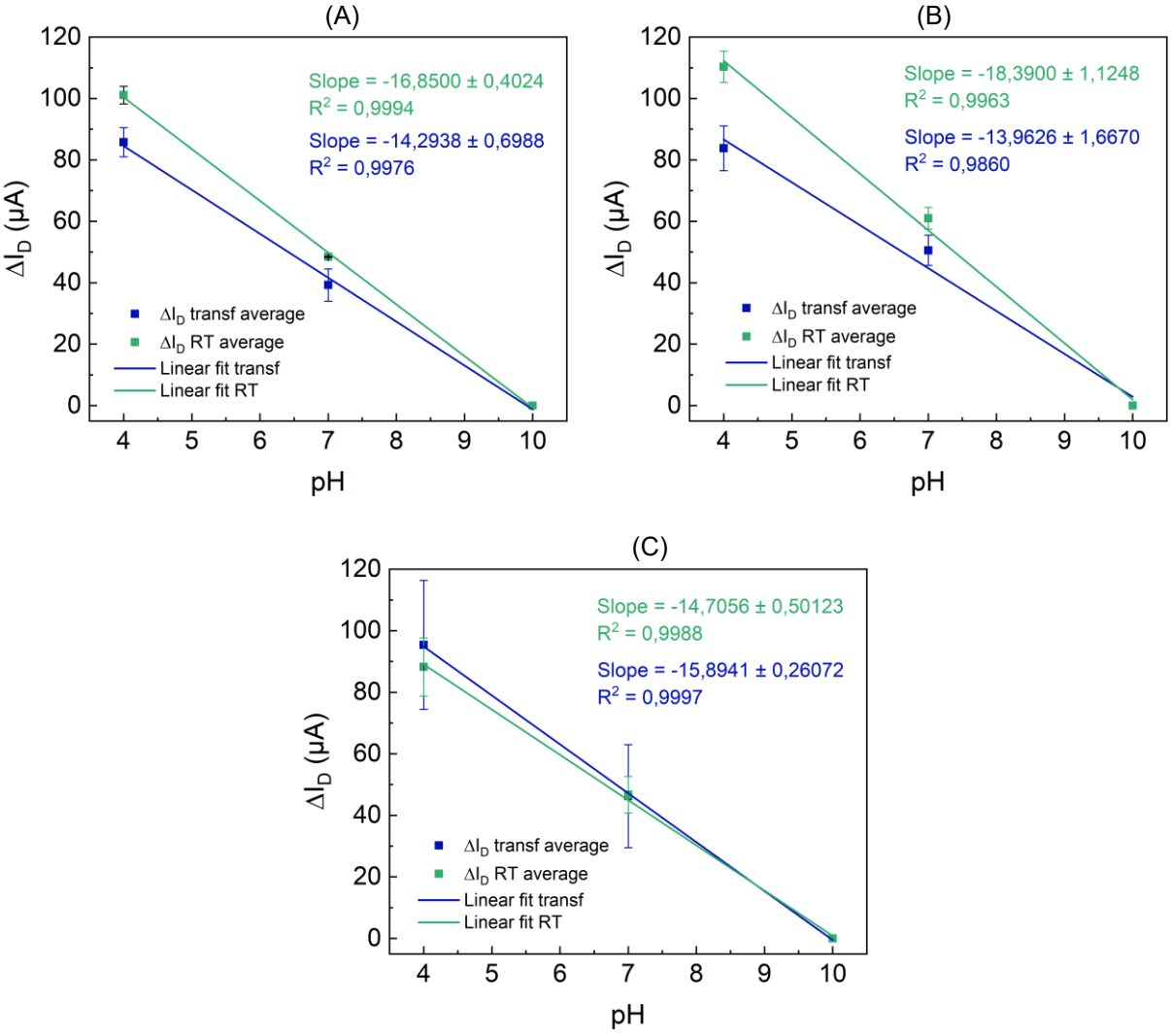

Figure 4.11 – Average pH sensing performance of sensors on PEN substrate: (A) sensor 1; (B) sensor 2; (C) sensor 3.

Comparing the results, if the sensitivity extracted from the real time measurements is taken as reference, it shows not only to be greater when directly compared with the sensitivity expressed by the same units extracted from the transfer characteristics, but also shows a greater signal to error ratio in relation to the other two sensitivity extraction methods. These results show the real time measurement method to be more precise, following a more linear trend for the data collected on the three pH buffer solutions used to test the sensors performance. Real time monitoring results also showed less deviation in between cycles when directly compared to the results obtained by extracting the transfer characteristics. Moreover, real time monitoring allows for an increase in the temporal resolution of measurements since it is possible to choose a frequency of data acquisition. Subsequently, effects like drift and hysteresis are easier to percept when testing sensors via real time monitoring. All of this while avoiding unnecessary stress inducement in the MOSFET which affects the precision of the measurements.

Table 3 - Summary of the results obtained for each tested sensor fabricated on PEN and CelSmartSense with coating substrates.

Substrate	Tested sensor	Sensitivity [µA/pH][1]	Sensitivity [µA/pH][2]
PEN	Sensor 1	14.3 ± 0.7	16.9 ± 0.4
	Sensor 2	14.0 ± 1.7	18.4 ± 1.1
	Sensor 3	15.9 ± 0.3	14.7 ± 0.2
	Average	14.2 ± 0.2	16.9 ± 1.0
CelSmartSense w/ coating	Sensor 1	13.4 ± 1.2	18.4 ± 1.4
	Sensor 2	21.0 ± 1.3	17.6 ± 0.3
	Sensor 3	11.2 ± 0.3	17.5 ± 1.0
	Average	15.5 ± 3.4	17.7 ± 0.4

[1] Sensitivity extracted from transfer characteristics; [2] Sensitivity extracted from real time monitoring.

The sensitivities obtained through the average values of each individual tested sensor from the batches produced on PEN and CelSmartSense substrates reveal higher average sensitivities are obtained with the real time monitoring measurement methodology. In terms of signal to error ratio, sensors on PEN substrate do not show an increase, however, sensors on CelSmartSense paper showed a very significant increase of signal to error ratio from 4.5 to 41.2 which translates into an enhancement of 800% in signal to error ratio when referring to real time monitoring of the drain current. To make sure that the tendency was for the results be more precise when extracted from the real time monitoring method, sensors on corning glass were also tested. Results can be found in Appendix A.5, where sensitivity results are 18.36 ± 2.05 µA/pH obtained from transfer characteristics versus 20.49 ± 1.58 µA/pH obtained from real time monitoring. With this the confirmation is made that real time monitoring shows results with greater sensitivities and overall lower associated error, thus enhancing the signal to error ratio of sensor testing. For the reasons shown and discussed, real time monitoring was selected as the optimal method for the signal detection of the sensors.

4.2 Sensors on cellulose-based substrates

In this sub-chapter the performance of sensors produced on cellulose-based substrates is discussed through the optimized detection protocol established. The premise of this analysis was to see what performance one could get from CMISFET devices produced on cellulose-based substrates. Firstly, checking the dry performance to see if a capacitive structure is conserved during production. After this, a buffer solution was placed in contact with the sensitive area and a performance test of the sensors conducted to see if a paper without a special post coating process (CelSmartSense without coating) could function in contact with test solutions and in a positive case, directly compare them with the produced sensors on CelSmartSense paper with ethyl cellulose coating. Other comparison of interest was established between the sensors on Whatman paper, which does not have any fiber refining process to smoothen the surface versus the CelSmartSense ones.

Results are compared between sensors on paper substrates and in the end a final comparison is performed regarding the performance of sensors on cellulose-based substrates versus the sensors produced on reference substrates, in order to infer about the possibility of substituting the established polymer-based matrixes for the production of these sensors and use in practical applications.

4.2.1 Preliminary capacitance tests

Firstly, the batches of sensors produced where submitted to a dry capacitance test in order to assess the percentage of working sensors. As cellulose-based substrates show much more surface roughness, this was a starting point to compare the different batches produced and check the influence of surface treatments and coatings on the thin films that make the capacitor's structure (Mo contacts and Parylene-C dielectric). The obtained averages for the capacitance of each batched produced are shown in Table 4, where results indicate that the majority of the sensors were working and had comparable capacitances to the ones obtained for the reference batch produced on a corning glass substrate (batch capacitance shown in Appendix A.6). However, it is noticeable that the batch of sensors on Whatman paper substrate had the highest percentage of sensors in which the capacitor was not working properly. This can be related to the roughness of the substrate which does not allow for an optimal adhesion of the thin films deposited by vapour deposition techniques. On CelSmartSense substrates, an increase of working sensors of approximately 20% may indicate that a fiber refining process is important to decrease the surface roughness and promote a better adhesion of thin films, which in the end results in more consistent and conformable devices. Moreover, the ethyl celulose layer deposited as post coating, did not seem to affect the adhesion of thin film layers, since a high yield of working sensors was obtained with a low standard deviation of nominal capacitance.

Table 4 – Average batch capacitances and percentage of working sensors fabricated on cellulose-based substrates.

Substrate	Average batch Capacitance [nF]	Percentage of working sensors
Whatman w/coating	0.20 ± 0.03	60 %
CelSmartSense w/coating	0.16 ± 0.06	80%
CelSmartSense w/o coating	0.22 ± 0.26	76%

4.2.2 Absorption tests

The major drawback of sensors on cellulose-based substrates was the absorption of the liquid medium in direct contact with the sensitive area of the sensors.

Before conducting the measurements protocol on each sensor, all substrates were submitted to an absorption test, exposing the Ta_2O_5 sensitive area to pH10 buffer solution while having the sensors connected to the measurement setup in a closed environment to avoid unwanted evaporation of the solution. The initial moment after pipetting the liquid sample onto the sensitive area was captured versus the moment where the majority of the liquid sample had been absorbed and the drain current signal started to shift from its original stabilized value. More in depth hydrophobicity tests could have been conducted for each substrate, measuring the exact contact angle, however, for simple objective of observing if the substrate would allow the sensing electrode to operate properly, this analysis was sufficient. Absorption was more accentuated on CelSmartSense substrate without coating, which showed almost immediate absorption of the liquid medium and consequent degradation of the electrical signal under 5 minutes of being exposed to it. Therefore, this sensor did not allow to conduct the measurement protocol. Whatman paper substrate with coating showed an identical issue, with absorption of the majority of the liquid samples after 15 minutes. CelSmartSense substrate with coating showed the best isolation against a liquid analyte, lasting more than 45 minutes without fully absorbing the liquid samples pipetted on the sensitive area. Despite absorption of the liquid samples, all tested sensors on cellulosed based substrates did not show any exterior signs of degradation of the sensing structure over the testing cycles nor did their performance in terms of sensitivity seemed to diminish. The absorption behaviour recorded on the tested sensors is shown in Figure 4.12.

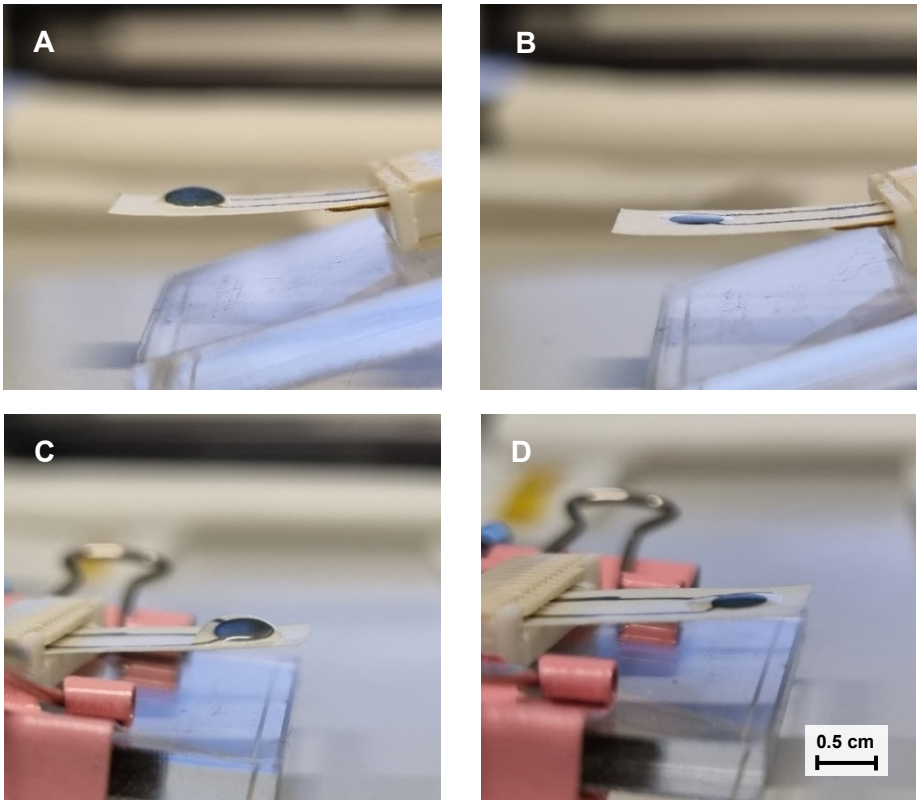

Figure 4.12 – Images captured on sensors on cellulose-based substrates. (A and B) Liquid sample on Whatman substrate with ethyl cellulose coating at 0 min vs after 15 min when drain current I_D started shifting from the stabilized value. (C and D) Liquid sample on CelSmartSense substrate with ethyl cellulose coating at 0 min vs after 45 min when drain current I_D started shifting from the stabilized value.

Images for the sensor on CelSmartSense substrate without coating could not be recorded, however in the recording of the drain current I_{DS} for each substrate, shown in Figure 4.13, it is possible to analyse the behaviour of the sensors on the different cellulose-based substrates when exposed to the analyte. The current intensity is constant throughout a given time, for each substrate, until the liquid sample is fully absorbed, and I_{DS} drops to the current associated to the control voltage (V_C). From these results, it is possible to conclude that the ethyl cellulose coating layer is crucial to create a needed isolation of the device, providing a hydrophobic protecting layer that impermeabilizes the substrate, keeping liquid mediums from absorbing further into the substrate and device's structure. However, Whatman substrate with coating was not able to maintain the liquid solution for more than 15 minutes in average, compared to an average of 45 minutes of the CelSmartSense substrate with coating, while keeping a stabilized current output. This can be related to the fiber refining process to reduce surface roughness, carried for CelSmartSense substrates. This process proves to be necessary, because achieving lower surface roughness promotes a better adhesion of the ethyl cellulose coating. The performance in time (~3000 s) achieved by sensors on CelSmartSense substrate with coating in direct contact with a buffer solution allows for the use of such devices in the majority of applications in the context of chemical and biochemical solution sensing. This type of integrated reactions for analyte detection occurs with fast kinetics, with duration typically bellow 30 to 45 minutes. Nevertheless, sensors on Whatman substrate with coating were still tested to be directly compared with the sensors on CelSmartSense substrate with coating. Both were submitted to the pH testing protocol defined in chapter 3.

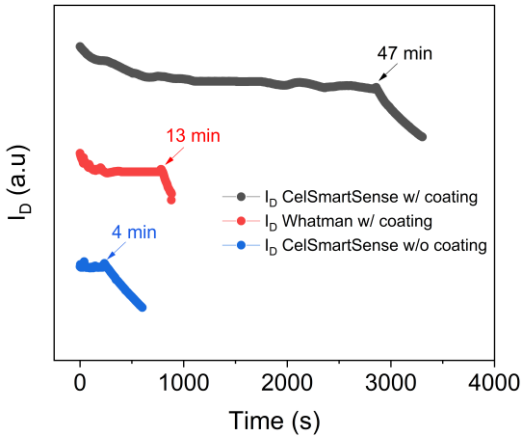

Figure 4.13 – Shifting of the drain current I_{DS} after absorption of pH 10 buffer solution in contact with the sensitive area of sensors fabricated on cellulose-based substrates.

4.2.3 pH sensing performance

The optimized detection protocol concluded in the previous subchapter was used to extract, evaluate and compare the performance of the sensors produced on cellulose-based substrates with an ethyl cellulose coating layer. As referred, the sensitive area of the sensors was exposed to constant ionic strength buffer solutions of different pH. In Figure 4.14 A and B, the real time monitoring of a cycle for tested sensors on Whatman and CelSmartSense papers with ethyl cellulose coating are respectively shown. The exhibited behaviours were a staple for the majority of sensors tested out of each batch. The noted absorption on Whatman paper substrate had an implication on the device's performance. As it is possible to see a significant difference in the stabilization of the drain current for each pH buffer solution from the real time cycles performed on both batches of sensors. Sensors on Whatman paper showed initial values of drain current for each pH that were in line with the ones obtained with sensors on CelSmartSense, however due to the constant absorption and need to pipette new solution to run the tests, the performance is degraded. By having more absorption of the liquid medium, an hysteresis effect was constant and thus the change in solution throughout the cycles was not very effective,

leading to an increasing stabilization time. This was evidenced from the duration of a full cycle, which was in average two to three times longer than a cycle performed on sensors of the CelSmartSense with coating batch.

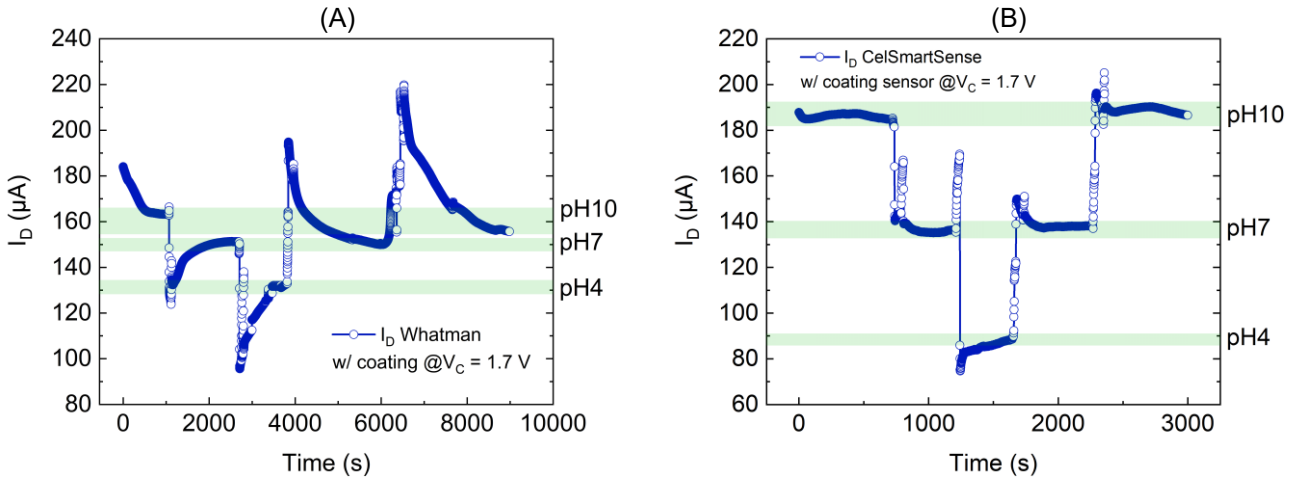

Figure 4.14 - CMISFET pH sensing performance of sensors on cellulose based substrates through real time monitoring of the drain current I_{DS} at a control voltage of V_C = 1.7 V: (A) real time cycle of a sensor on Whatman paper substrate; (B) real time cycle of a sensor on CelSmartSense with coating paper substrate. Noting the difference on the x-axis time scale.

Following these measurements of three real time monitoring cycles for three sensors of each batch, the analysis protocol was carried out in order to establish a comparison of both batches of sensors and also between the other reference devices fabricated on PEN and corning glass substrates.

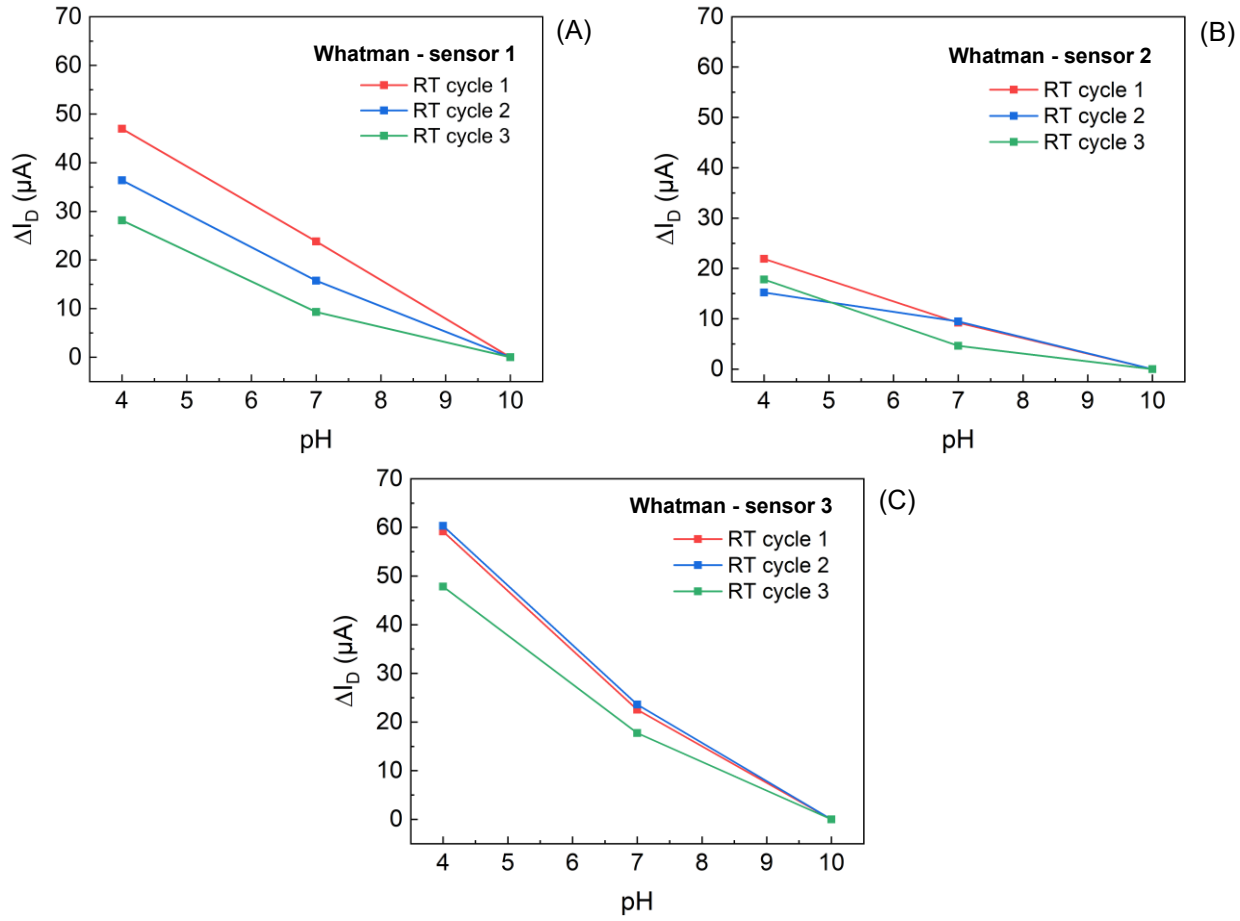

Figure 4.15 - Sensitivity analysis of the tested sensors on Whatman paper substrate with ethyl cellulose coating. Results extracted from the real time continuous monitoring of the drain current I_{DS} for the three tested sensors. (A) sensor 1; (B) sensor 2; (C) sensor 3. Connecting lines are a mere representation of the sensitivity tendency between data points.

The results obtained for the three tested sensors on Whatman paper substrate with coating are depicted in Figure 4.15. Results of the tested sensors CelSmartSense with coating batch are shown in Figure 4.16. Comparing both results it is clear the sensitivities obtained for the Whatman batch of devices are in general much lower than the ones obtained in the tested CelSmartSense with coating batch. Standard deviations of the drain current transduced for each pH solution tested similar absolute value for both sensors. However, since CelSmartSense sensors show much higher absolute differences ΔI_D (pHx-pH10), the signal to error ratio is notoriously higher.

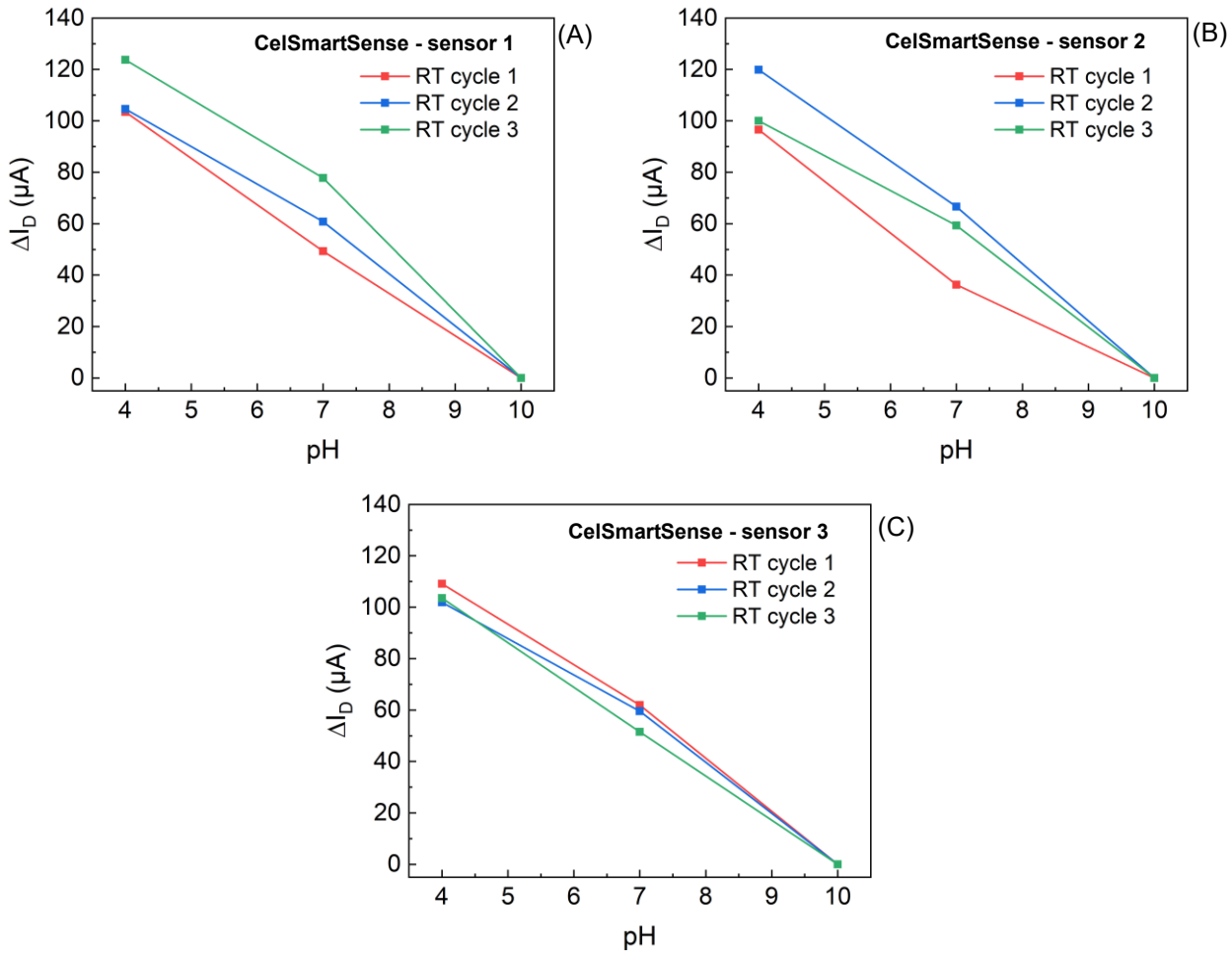

Figure 4.16 - Sensitivity analysis of the tested sensors on CelSmartSense paper substrate with ethyl cellulose coating. Results extracted from the real time continuous monitoring of the drain current I_{DS} for the three tested sensors. (A) sensor 1; (B) sensor 2; (C) sensor 3. Connecting lines are a mere representation of the sensitivity tendency between data points.

In order to have a clear view of the average sensitivities and the relative errors associated with each pH solution in between cycles, the data was plotted for all the tested sensors. Results obtained for the batches of sensors on Whatman and CelSmartSense paper substrates with coating are shown in Appendix A.4. From these results it is possible to see from the depicted performance of each sensor for the two tested paper batches, the sensitivity of the sensors on CelSmartSense paper with coating is for all sensors about three to four times higher compared to the sensors from the Whatman paper batch. Another evidence is the variability of performance in between sensors, which is far higher for sensors on Whatman paper, as it is possible to see by the different slopes shown on each plot. Analysing each sensor individually, it is clear that for both batches there is an inherent relative error associated with pH measurements. This error in ΔI_D reaches 15 μA in the case of sensors on Whatman paper and a maximum of 24 μA for the pH7 associated measurements in the second tested sensor of the CelSmartSense batch, which becomes a problem if, for other pH's there is also a considerable relative error, and if the absolute shift is too large, it may result in an inability to reliably distinguish solutions

for a given measurement. This tendency was more evident for the pH7 associated measurements, where deviations are directly influenced by the hysteretic behaviour felt in the real time monitoring for the pH7 associated drain current stabilization levels, associated to steps of pH7 → pH4 → pH7. These results are outlined in average sensitivity obtained from the three tested sensors of each batch, depicted in Figure 4.17.

Table 5 - Summary of the results obtained for each tested sensor fabricated on Whatman and CelSmartSense paper substrates with coating.

	Tested sensor	Sensitivity from RT measurements [µA/pH]
Whatman paper w/ coating	Sensor 1	6.2 ± 0.4
	Sensor 2	3.1 ± 0.3
	Sensor 3	9.3 ± 1.3
	Average	7.7 ± 1.6
CelSmartSense w/ coating	Sensor 1	18.4 ± 1.4
	Sensor 2	17.6 ± 0.3
	Sensor 3	17.5 ± 1.0
	Average	17.8 ± 0.4

Between the batches of sensors on Whatman and CelSmartSense papers with coating a performance difference in sensitivity is clearly noted. Sensors on CelSmartSense showed a sensitivity three times higher than the sensors on Whatman substrate. Moreover, the error associated with the displayed data, showed to be six times lower for ΔI_D pH4 and about 2 times lower for ΔI_D pH7. This was no surprise since most of the tested sensors from the CelSmartSense with coating batch showed very small standard deviations associated with each pH, while the constant abosrption occuring for sensors on Whatman substrates created a degradation of the results over cycles, which lead to a much higher variability of the output of this sensors.

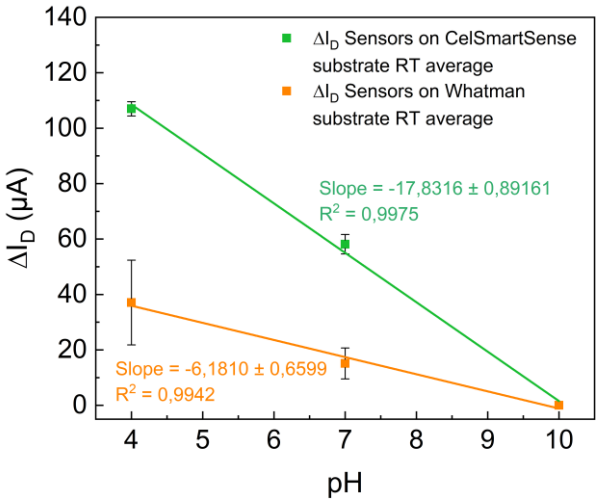

Figure 4.17 – Sensitivity comparison of sensors on cellulose-based substrates. Green dots represent the average values from all tested sensors produced on CelSmartSense substrate with coating while orange dots represent the average results of the sensors produced on Whatman paper substrate with coating.

Average results obtained for the tested sensors on paper substrates are shown Table 6, alongside with the results obtained for sensors produced on corning glass and PEN substrates, in order to establish a direct comparison in terms performance. Despite the transfer characteristics not being the chosen methodology of analysis for data comparison, sensitivity in mV/pH and µA/pH extracted through this methodology is only shown to have a better visualization of the general scenario for all the tested sensors and also due to sensitivity in mV/pH comes as the most common performance units used in literature to establish comparisons related with the sensor's sensitivity.

Table 6 – Summary of CMISET sensors performance on all tested substrates.

Substrate	Sensitivity [mV/pH][1] for constant I_{ref}	Sensitivity [µA/pH][1] for constant V_{ref}	Sensitivity [µA/pH][2]	Hysteresis [µA]	Average RT cycle duration [s]
Corning glass	33.2 ± 2.8	18.4 ± 2.0	20.5 ± 1.6	6.2	~ 3800
PEN	27.7 ± 2.0	14.2 ± 0.2	16.9 ± 1.0	8.1	~ 4800
CelSmartSense w/o coating	n.d*	n.d*	n.d*	n.d*	n.d*
CelSmartSense w/ coating	31.7 ± 6.3	15.5 ± 3.3	17.8 ± 0.4	11.2	~ 5400
Whatman w/ coating	14.3 ± 2.3	6.2 ± 1.2	7.7 ± 1.6	15.4	~ 10100

[1] Sensitivity extracted from transfer characteristics; [2] Sensitivity extracted from real time monitoring.

* Non defined - it was not possible to measure sensors on CelSmartSense substrate without ethyl cellulose coating. When in contact with the liquid samples, sensors showed immediate absorption.

With this summary of data another comparison was performed for the sensors on cellulose-based substrates, regarding the average duration of a real time cycle. Sensors on CelSmartSense with coating showed a full real time monitoring cycle of half the time when compared to the one obtained for the sensors on Whatman paper, which indicates that devices fabricated on CelSmartSense substrate with coating have a much more effective charge inducing mechanism takes place. This again due to the enhanced properties achieved by a fiber refining process to smoothen the substrate surface before applying the ethyl cellulose coating. Now comparing the performance of sensors on paper substrates, having the CelSmartSense batch with coating as example, with the sensors produced on the reference substrates, it is seen that through the optimized measurement protocol using the real time monitoring as the preferential signal extraction method, the sensitivity average of the paper substrate is very comparable to the ones of sensors on corning glass and PEN. Moreover, by establishing a comparison solely in between signal to error ratios, sensors on CelSmartSense substrate with coating shows the highest SER = 41.8 in relation to SERs of about 20 for the other two batches of sensors produced. Moreover, the average real time cycle duration is comparable between substrates, having as expected the sensors on corning glass as the fastest to stabilize the inducing mechanism for a complete cycle of changing buffer solutions and PEN and CelSmartSense following in this order, both with very close full cycle times. This way it is possible to conclude that sensors fabricated on a paper substrate such as CelSmartSense with ethyl cellulose coating can exhibit a performance close to sensors on other substrates. It was not possible to identify

comparable cellulose-based devices in literature, however framing the results exhibited in this work with other ISFET devices reported in literature presented in chapter 1, the sensitivity, hysteresis, and overall reproducibility, the results are very promising.

5 Conclusions and future perspectives

Sensors were produced in a total of four different substrates: corning glass, polyethylene naphthalene (PEN) and two cellulose-based substrates – Whatman and CelsmartSense papers, to establish a comparison in terms key sensor properties such as sensitivity and stability. Moreover, cellulose-based substrates were introduced, reportedly for the first time for this sensor architecture, with the objective of having a more eco-friendly and altogether less expensive fabrication route.

A more refined measurement and data analysis protocol was developed in order to test the sensors performance and establish a direct comparison between sensors of different batches and fabricated on different substrates. Moreover, an inverted connection topology was tested for this architecture for both PEN and cellulose-based substrates, having the control voltage applied to the top Mo contact and thus having charge inducement at the bottom electrode, which is connected to the MOSFET gate, as opposed to the standard connection topology used in the past. Results using this new approach resulted an increase in sensitivity of 200-300% for both measurement methodologies, while keeping an identical relative error. With this inverted connection topology, real time monitoring results showed overall lower noise, and stabilization of the drain current for each pH buffer solution was about 1.7 times faster compared to using the standard approach. Moreover, results obtained with the inverted connection topology tended to be more linear throughout the tested pH range, as shown by the R^2 coefficient of the linear fits performed. Here, having the control voltage applied directly under the sensitive area affects the electrophoretic mechanism of charge induction. The approximation of ionic charges to the sensitive surface seems to be no longer ruled by the pKa of the oxide material, but instead forced by the superimposed potential applied underneath the sensitive layer. This enhanced the charge inducing process, but more practical tests need to be conducted to sustain conclusions on the electrochemical phenomenon behind this effect.

Tests conducted using both measurement methodologies indicate that real time monitoring of the drain current I_{DS} is a more accurate and reliable data acquisition method over the transfer characteristics extraction, returning higher sensitivities with less I_D(pHx) associated error between cycles, thus higher signal to error ratios.

Regarding the performance of sensors on cellulose-based substrates, the sensors were first compared via dry capacitance testes, without any liquid sample in contact with the sensitive area. Results were indicative of a lower percentage (60%) of working sensors for the batch produced on Whatman paper substrate compared to ~80% of working sensors on both batches of sensors fabricated on CelSmartSense paper substrates.

The clear problem of the sensors on cellulose-based substrates was the absorption of the liquid medium which was in direct contact with the sensitive area of the sensors. These tests were also to check if there was any noticeable degradation of the device layers, as a result of expansion of the paper fibres upon absorption of the liquid medium. This problem was more accentuated on CelSmartSense substrate without coating, which showed absorption of the liquid medium in under 5 minutes of being exposed to it. Whatman paper substrate with coating showed an identical behaviour, with absorption of the majority of the liquid samples after 15 minutes. CelSmartSense substrate with coating showed the best impermeability overall, withstanding more than 45 minutes without fully absorbing the liquid samples pipetted on the sensitive area while keeping a constant output of current. Despite absorption of the liquid samples, all tested sensors on cellulosed based substrates did not show any exterior signs of degradation of the sensing structure over the testing cycles nor did their performance in terms of sensitivity seemed to diminish. This was a proof that the ethyl cellulose coating is crucial to impermeabilize the surface. Moreover, the performance comparison of sensors produced on both Whatman and CelSmartSense papers with ethyl cellulose coating, provided evidence that supported

the need of fiber refining processes, which reduces surface roughness of the paper and promotes a better adhesion of the ethyl cellulose coating.

pH performance of sensors on cellulose-based substrates was assessed and compared via the established optimal measurement protocol, with the control voltage applied on the top electrode and extracting the current I_D through real time continuous monitoring. Sensors on CelSmartSense substrate with coating showed the best performance with an average sensitivity of 17.8 ± 0.4 μA/pH compared to 7.7 ± 1.6 μA/pH obtained for sensors on Whatman substrate with coating. Besides, the performance of sensors on CelSmartSense substrate could match that of sensors produced on reference substrates such as corning glass (20.5 ± 1.6 μA/pH) or PEN (16.9 ± 1.0 μA/pH), while showing a similar time for the stabilization of the charge inducing mechanism. In conclusion, sensors on a cellulose-based substrate with a surface smoothening pre-treatment and a final coating process to isolate and concede hydrophobicity to the surface, such as CelSmartSense with ethyl cellulose coating can show identical performance when compared to reference substrates such as PEN and glass, with the advantage of being an eco-friendly alternative and altogether less expensive to produce. Moreover, the frame of results obtained for the several substrates were identical, which indicates the production and sensor measurement protocols were robust enough to compare sensors produced on different substrates.

Moving forward, and in order to further complement and improve the CMISFET architecture for use in a wide range of sensing applications, especially for the ones where more demanding in terms of accuracy, some implementations are discussed:

- The data analysis protocol, carried out for comparison of the sensors on different substrates was no more than a differential approach of data extraction, with reference to the pH10 associated drain current. Compared to the bulk data extracted, using this method reduces variability over the cycles, improving signal to error ratio. In a practical scenario, this would translate in no more than a differential sampling sensing matrix, with one sensor having its sensitive area exposed to the aqueous solution and the other fully encapsulated serving as a reference. This would minimize the common mode signal which can have a significant impact on measurements.
- In order to diminish I_D(pHx) errors associated with the hysteresis verified on the real time measurements, which result of the accumulation of charges when exposed to the same solution for an extended period, an opposite voltage (negative) may be applied to the control gate. This would invert the polarity of the electric field the interface was constantly submitted to and force the release of accumulated charges at the interface. The magnitude of the applied voltage would need to be tested to check if there were to be any unintentional stress induced on the sensitive area interface.
- Objective of a later substitution of the commercial MOSFET used with an oxide-TFT-based front-end conditioning circuit, not only to amplify the signal but also to reduce noise sources and provide a clean output for subsequent digitalization.

References

[1] "Global Biosensors Market Report 2022-2035: $1.2 Billion." https://www.globenewswire.com/en/news-release/2022/07/26/2485813/28124/en/Global-Biosensors-Market-Report-2022-2035-1-2-Billion-Invested-in-the-Last-5-Years-with-Further-Growth-Expected.html (accessed Sep. 06, 2022).

[2] M. Waleed Shinwari, M. Jamal Deen, and D. Landheer, "Study of the electrolyte-insulator-semiconductor field-effect transistor (EISFET) with applications in biosensor design," *Microelectron. Reliab.*, vol. 47, no. 12, pp. 2025–2057, 2007, doi: 10.1016/j.microrel.2006.10.003.

[3] R. S. D. M. Valle, *Robotic Tactile Sensing.*, vol. 11, no. 1. 2013.

[4] Branquinho, R. M. M. S., "Label-free detection of biomolecules with Ta2O5 - based field effect devices.", 2012, PhD thesis, NOVA University FCT-UNL, Lisbon..

[5] S. M. Sze and K. K. Ng, *Physics of Semiconductor Devices: Third Edition*. 2006, ISBN: 1119618002, 9781119618003.

[6] B. Veigas, E. Fortunato, and P. V. Baptista, "Field effect sensors for nucleic acid detection: Recent advances and future perspectives," *Sensors (Switzerland)*, vol. 15, no. 5, pp. 10380–10398, 2015, doi: 10.3390/s150510380.

[7] P. Bergveld, "Development of an Ion-Sensitive Solid-State Device for Neurophysiological Measurements," in IEEE Transactions on Biomedical Engineering, vol. BME-17, no. 1, pp. 70-71, Jan. 1970, doi: 10.1109/TBME.1970.4502688.

[8] C. Toumazou *et al.*, "Simultaneous DNA amplification and detection using a pH-sensing semiconductor system," *Nat. Methods*, vol. 10, no. 7, pp. 641–646, 2013, doi: 10.1038/nmeth.2520.

[9] Y. K. Reshetnyak, A. Moshnikova, O. A. Andreev, and D. M. Engelman, "Targeting Acidic Diseased Tissues by pH-Triggered Membrane-Associated Peptide Folding," *Front. Bioeng. Biotechnol.*, vol. 8, no. April, pp. 1–9, 2020, doi: 10.3389/fbioe.2020.00335.

[10] E. Yang *et al.*, "Influence of culture media, pH and temperature on growth and bacteriocin production of bacteriocinogenic lactic acid bacteria," *AMB Express*, vol. 8, no. 1, 2018, doi: 10.1186/s13568-018-0536-0.

[11] C. Triandafillou and D. Drummond, "Live Cell Measurement of the Intracellular pH of Yeast by Flow Cytometry Using a Genetically-Encoded Fluorescent Reporter," *Bio-Protocol*, vol. 10, no. 12, pp. 1–14, 2020, doi: 10.21769/bioprotoc.3653.

[12] R. Gentili, R. Ambrosini, C. Montagnani, S. Caronni, and S. Citterio, "Effect of soil ph on the growth, reproductive investment and pollen allergenicity of ambrosia artemisiifolia l.," *Front. Plant Sci.*, vol. 9, no. September, pp. 1–12, 2018, doi: 10.3389/fpls.2018.01335.

[13] J. D. Müller *et al.*, "Metrology for pH measurements in brackish waters-part 1: Extending electrochemical pHT measurements of TRIS buffers to salinities 5-20," *Front. Mar. Sci.*, vol. 5, no. JUL, pp. 1–12, 2018, doi: 10.3389/fmars.2018.00176.

[14] I. Fakih *et al.*, "Selective ion sensing with high resolution large area graphene field effect transistor arrays," doi: 10.1038/s41467-020-16979-y.

[15] N. Moser *et al.*, "Complementary Metal−Oxide−Semiconductor Potentiometric Field-Effect Transistor Array Platform Using Sensor Learning for Multi-ion Imaging," *Cite This Anal. Chem*, vol. 92, p. 5285, 2020, doi: 10.1021/acs.analchem.9b05836.

[16] P. Bergveld, "Thirty years of ISFETOLOGY: What happened in the past 30 years and what may happen in the next 30 years," *Sensors Actuators B Chem.*, vol. 88, no. 1, pp. 1–20, Jan. 2003, doi: 10.1016/S0925-4005(02)00301-5.

[17] G. A. J. Besselink and P. Bergveld, "ISFET Affinity Sensor," *Affin. Biosens.*, vol. 7, pp. 173–186, 2003, doi: 10.1385/0-89603-539-5:173.

[18] S. V. Dzyadevych, A. P. Soldatkin, A. V. El'skaya, C. Martelet, and N. Jaffrezic-Renault, "Enzyme

biosensors based on ion-selective field-effect transistors," *Anal. Chim. Acta*, vol. 568, no. 1–2, pp. 248–258, 2006, doi: 10.1016/j.aca.2005.11.057.

[19] V. Pachauri and S. Ingebrandt, "Biologically sensitive field-effect transistors: From ISFETs to NanoFETs," *Essays Biochem.*, vol. 60, no. 1, pp. 81–90, 2016, doi: 10.1042/EBC20150009.

[20] C. O. Manlises, F. R. Cruz, W. Y. Chung, and A. Paglinawan, "Characterization of an ISFET with built-in calibration registers through segmented eight-bit binary search in three-point algorithm using FPGA," *J. Low Power Electron. Appl.*, vol. 7, no. 3, pp. 1–10, 2017, doi: 10.3390/jlpea7030019.

[21] B. Veigas, "Development of Field Effect sensors for gene expression analysis : Application to cancer diagnosis," March, 2016, PhD thesis, NOVA University FCT-UNL, Lisbon.

[22] M. Barbaro, A. Bonfiglio, and L. Raffo, "A charge-modulated FET for detection of biomolecular processes: Conception, modeling, and simulation," *IEEE Trans. Electron Devices*, vol. 53, no. 1, pp. 158–166, 2006, doi: 10.1109/TED.2005.860659.

[23] B. Veigas *et al.*, "Quantitative real-time monitoring of RCA amplification of cancer biomarkers mediated by a flexible ion sensitive platform," *Biosens. Bioelectron.*, vol. 91, no. October 2016, pp. 788–795, 2017, doi: 10.1016/j.bios.2017.01.052.

[24] B. McCormick and D. Sanders, *Electricity and magnetism*, vol. 24, no. 2. 2008.

[25] M. Martins and P. M. Costa, "The comet assay in Environmental Risk Assessment of marine pollutants: Applications, assets and handicaps of surveying genotoxicity in non-model organisms," *Mutagenesis*, vol. 30, no. 1, pp. 89–106, 2015, doi: 10.1093/mutage/geu037.

[26] P. K. Shin and T. Mikolajick, "Alkali- and hydrogen ion sensing properties of LPCVD silicon oxynitride thin films," *Thin Solid Films*, vol. 426, no. 1–2, pp. 232–237, 2003, doi: 10.1016/S0040-6090(03)00041-5.

[27] K. M. Chang, K.-Y. Chao, H. Y. Hsu, and M. C. Huang, "Ultra-Low Drift Voltage by Using Gate Voltage Control in Oxide-Based Gate {ISFET}," *{ECS} Trans.*, vol. 6, no. 19, pp. 11–29, 2008, doi: 10.1149/1.2831726.

[28] N. F. de Rooij and P. Bergveld, "The influence of the pH on the electrolyte-SiO2-Si system studied by ion-sensitive fet measurements and quasi-static C-V measurements," *Thin Solid Films*, vol. 71, no. 2, pp. 327–331, 1980, doi: https://doi.org/10.1016/0040-6090(80)90167-4.

[29] S. Sinha *et al.*, "Fabrication, Characterization, and Modeling of an Aluminum Oxide-Gate Ion-Sensitive Field-Effect Transistor-Based pH Sensor," *J. Electron. Mater.*, vol. 50, no. 12, pp. 7085–7097, 2021, doi: 10.1007/s11664-021-09220-z.

[30] T. Matsuo and M. Esashi, "Methods of isfet fabrication," *Sensors and Actuators*, vol. 1, pp. 77–96, 1981, doi: https://doi.org/10.1016/0250-6874(81)80006-6.

[31] J. Bausells, J. Carrabina, A. Errachid, and A. Merlos, "Ion-sensitive field-effect transistors fabricated in a commercial CMOS technology," *Sensors Actuators B Chem.*, vol. 57, no. 1, pp. 56–62, 1999, doi: https://doi.org/10.1016/S0925-4005(99)00135-5.

[32] R. Shyam *et al.*, "Irradiation induced modification of structural and optical properties of potassium sodium niobate thin films," *Appl. Phys. A*, vol. 126, no. 1, p. 1, 2019, doi: 10.1007/s00339-019-3176-6.

[33] J. V Pinto, R. Branquinho, P. Barquinha, E. Alves, R. Martins, and E. Fortunato, "Extended-Gate ISFETs Based on Sputtered AmorphousOxides," *J. Disp. Technol.*, vol. 9, no. 9, pp. 729–734, 2013, [Online]. Available: https://opg.optica.org/jdt/abstract.cfm?URI=jdt-9-9-729.

[34] T. Akiyama, Y. Ujihira, Y. Okabe, T. Sugano, and E. Niki, "Ion-sensitive field-effect transistors with inorganic gate oxide for pH sensing," *IEEE Trans. Electron Devices*, vol. 29, no. 12, pp. 1936–1941, 1982, doi: 10.1109/T-ED.1982.21054.

[35] A. Poghossian and M. J. Schöning, "Detecting Both Physical and (Bio-)Chemical Parameters by Means of ISFET Devices," *Electroanalysis*, vol. 16, no. 22, pp. 1863–1872, 2004, doi: https://doi.org/10.1002/elan.200403074.

[36] M. Chen, Y. Jin, X. Qu, Q. Jin, and J. Zhao, "Electrochemical impedance spectroscopy study of Ta2O5

based EIOS pH sensors in acid environment," *Sensors Actuators B Chem.*, vol. 192, pp. 399–405, 2014, doi: https://doi.org/10.1016/j.snb.2013.10.129.

[37] Y. H. Pai, C. C. Chou, and F. S. Shieu, "Preparation and optical properties of Ta2O5-x thin films," *Mater. Chem. Phys.*, vol. 107, no. 2–3, pp. 524–527, 2008, doi: 10.1016/j.matchemphys.2007.08.032.

[38] J. C. Kim, J. S. Heo, Y. S. Cho, and S. H. Moon, "Atomic layer deposition of an HfO2 thin film using Hf(O-iPr)4," *Thin Solid Films*, vol. 517, no. 19, pp. 5695–5699, 2009, doi: 10.1016/j.tsf.2009.02.115.

[39] J. C. Chou and L. P. Liao, "Study on pH at the point of zero charge of TiO2 pH ion-sensitive field effect transistor made by the sputtering method," *Thin Solid Films*, vol. 476, no. 1, pp. 157–161, 2005, doi: 10.1016/j.tsf.2004.09.061.

Appendix

A.1 Physical masks used for thin film deposition

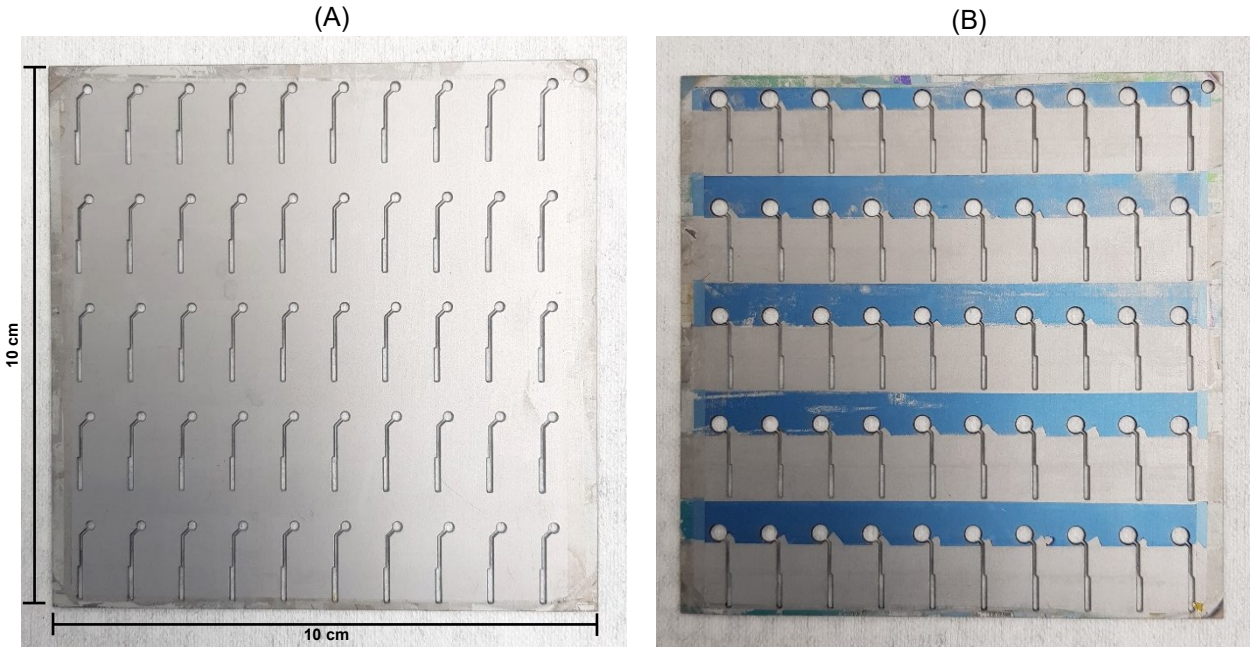

Figure A.1 – Physical masks used for sensors fabrication. (A) mask for bottom Mo contact layer deposition. (B) mask for bottom Mo contact and sensitive Ta_2O_5 layer depositions.

A.2 Sensors batches

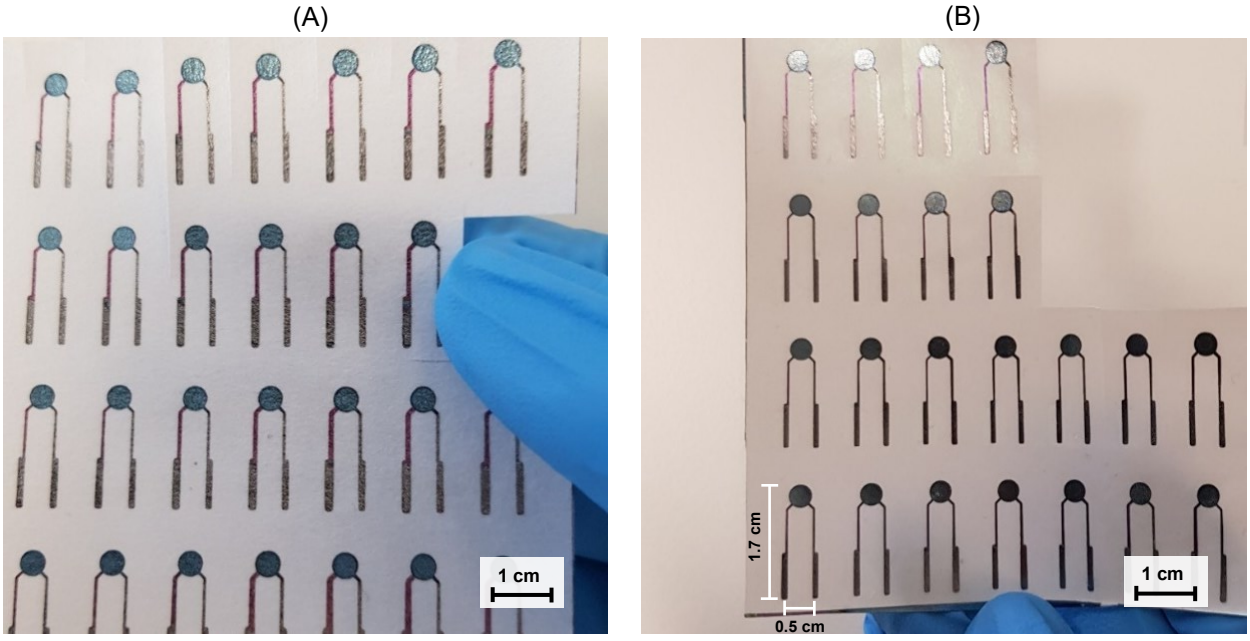

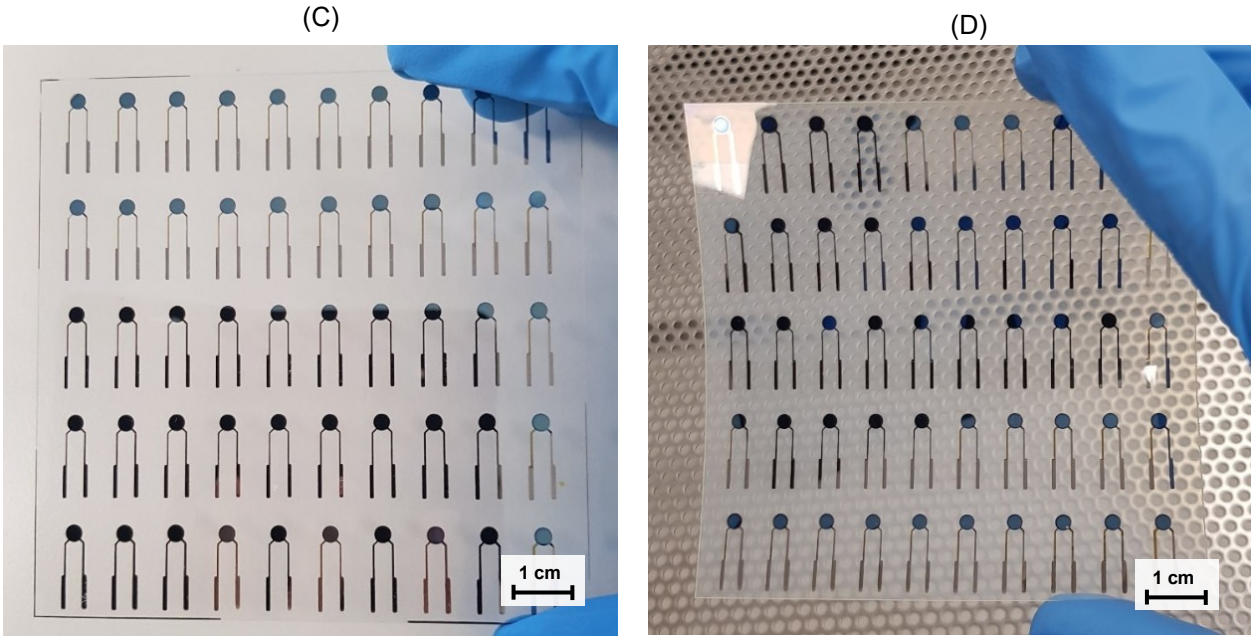

Figure A.2 – Batches of sensors produced. (A) batch produced on Whatman paper substrate with ethyl cellulose coating. (B) batch produced on CelSmartSense paper with coating. (C) batch produced on Corning glass substrate. (D) batch produced on PEN substrate.

A.3 Sensors testing setup

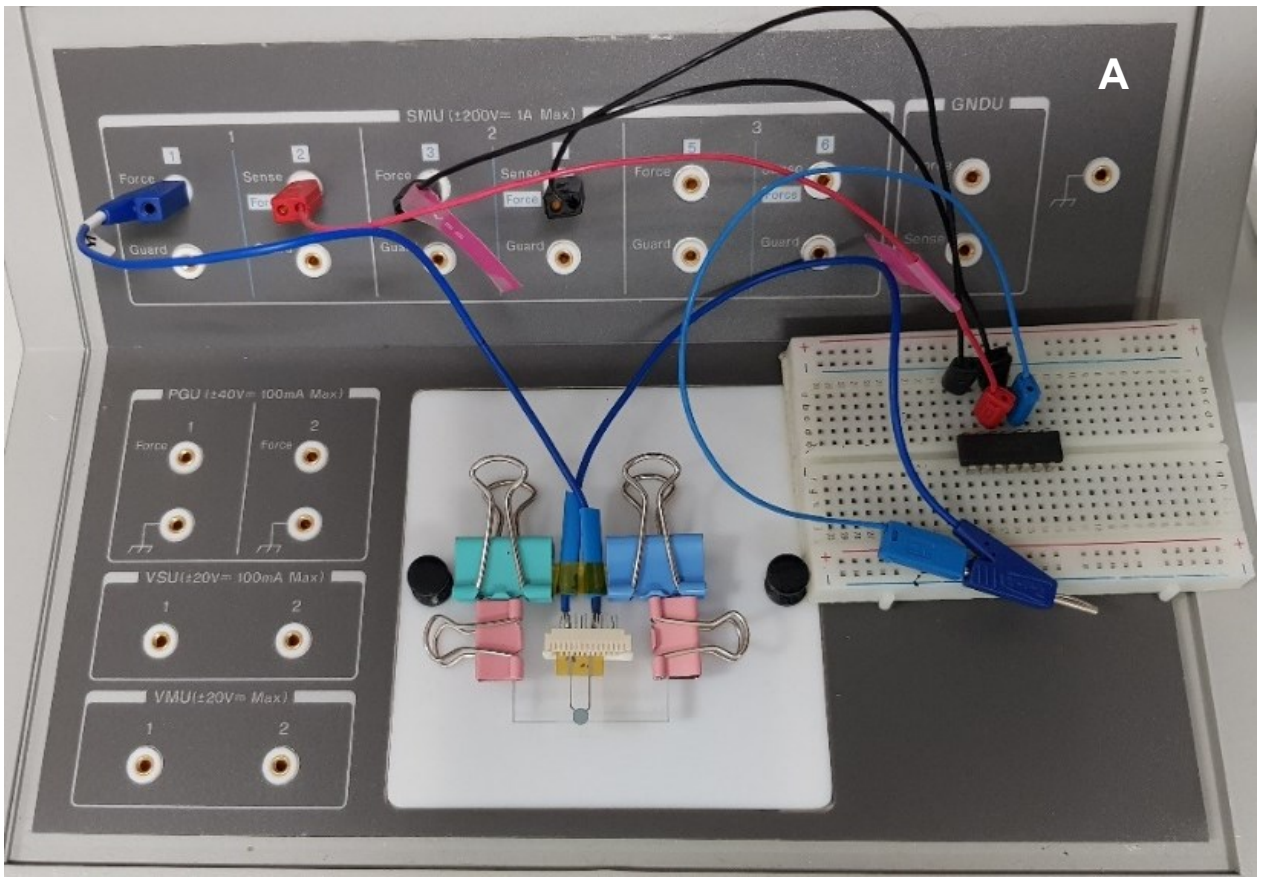

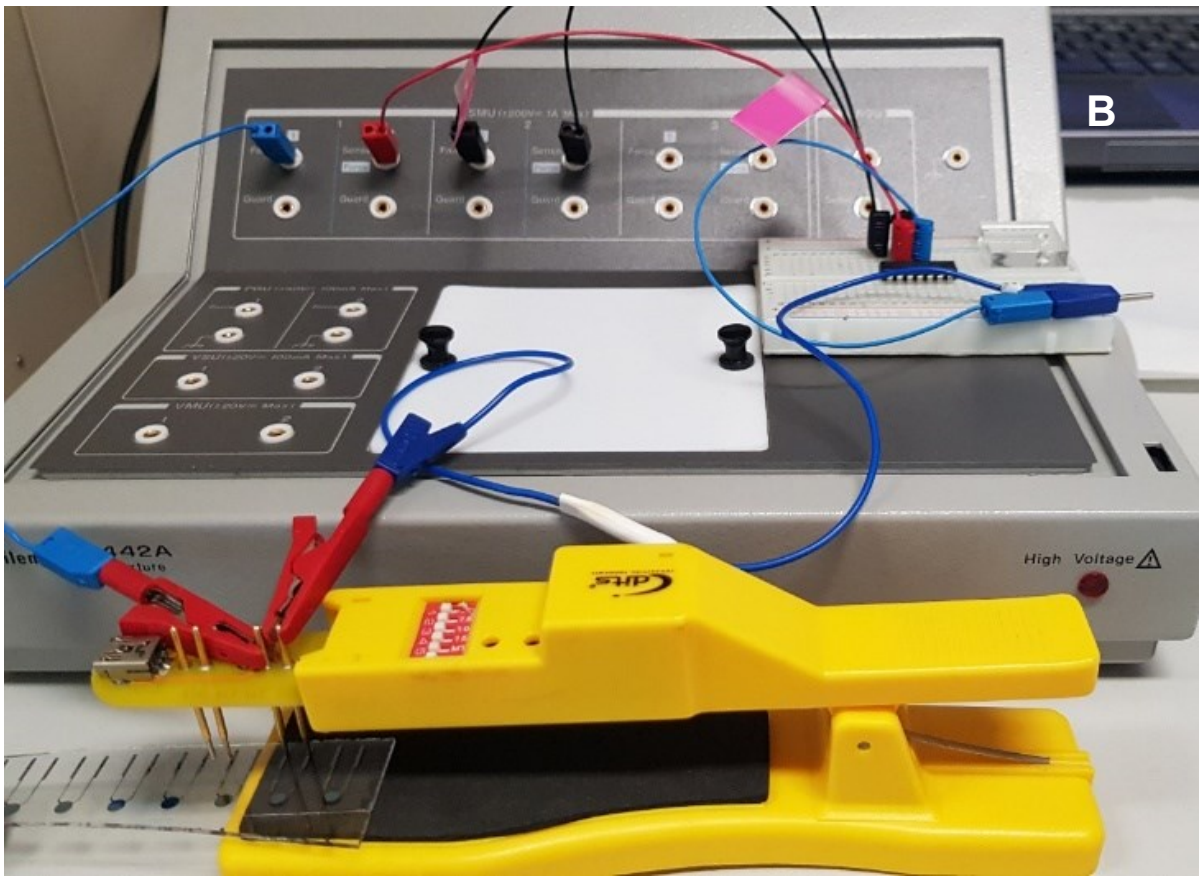

Figure A.3 – CMISFET measurements setup. (A) setup used for to test the sensors produced on cellulose-based and PEN substrates. (B) setup used to test the sensors produced on Corning glass substrate.

A.4 Sensors on cellulose-based substrates

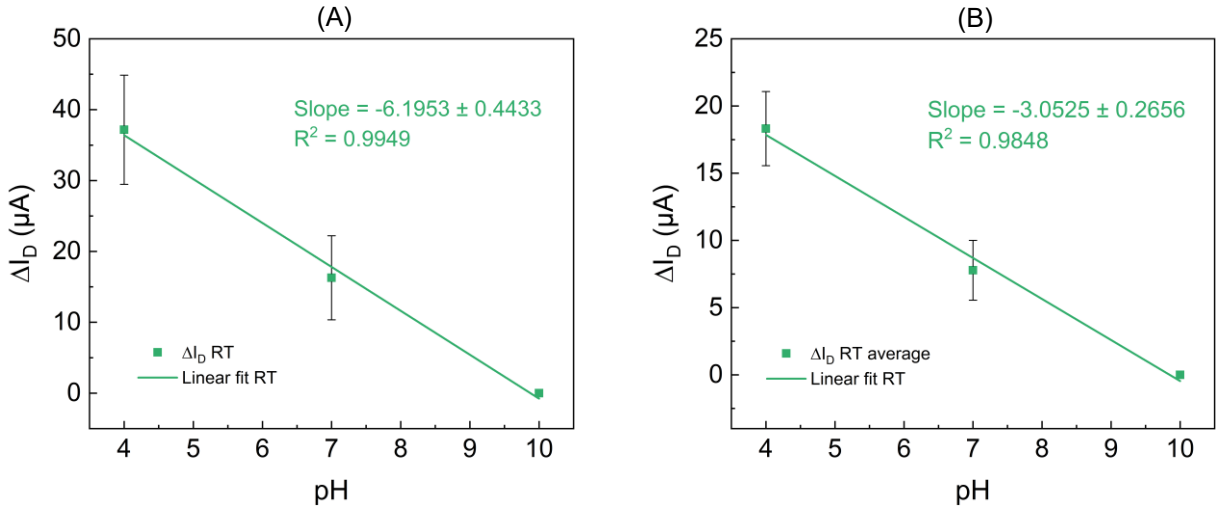

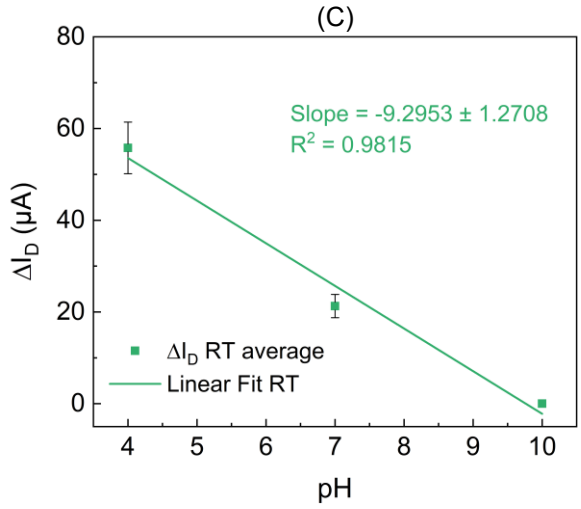

Figure A.4 - pH sensing performance of sensors on Whatman paper substrate. Average sensitivities obtained through real time monitoring of the drain current I_D for (A) sensor 1; (B) sensor 2; (C) sensor 3.

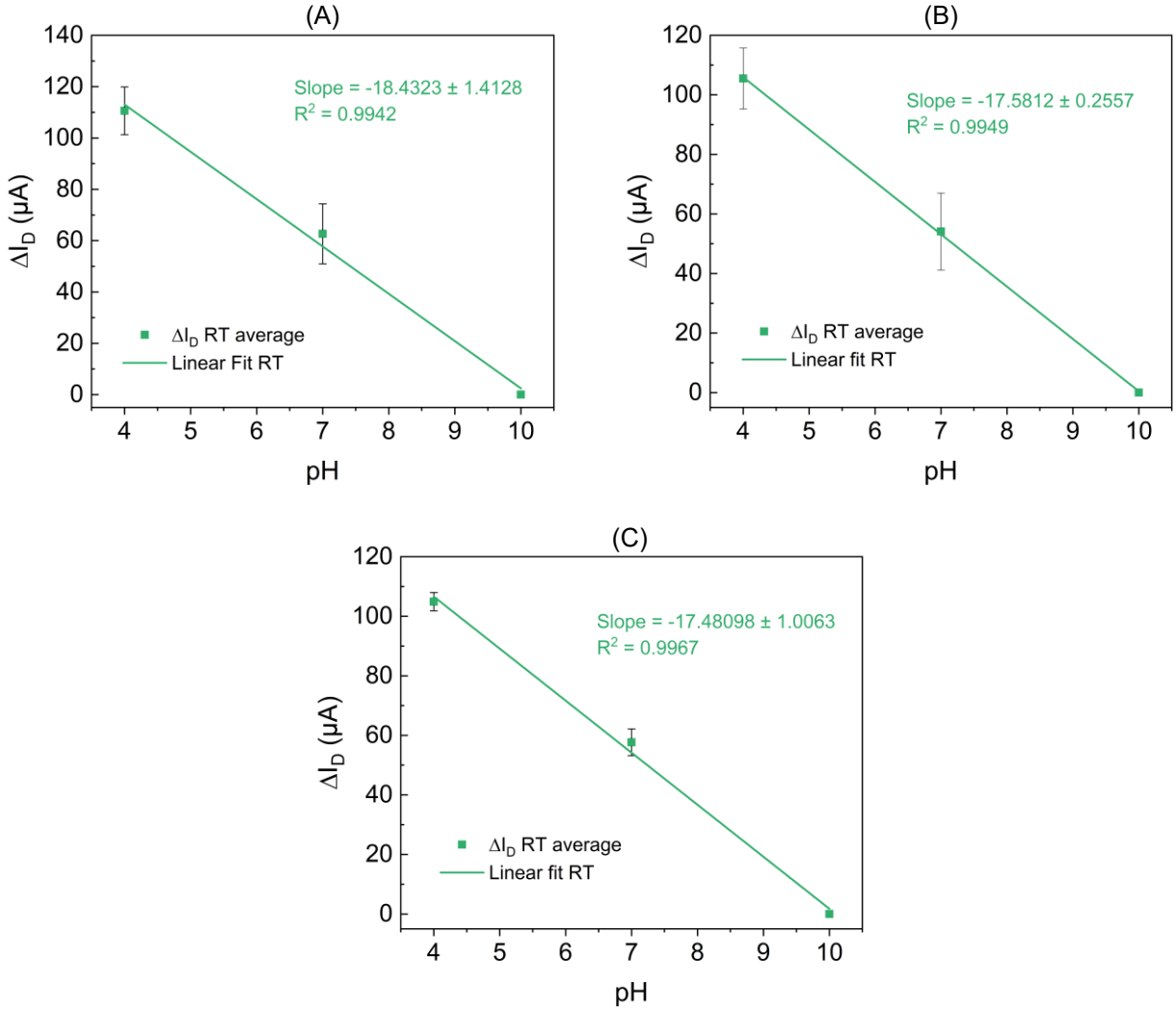

Figure A.5 - pH sensing performance of sensors on CelSmartSense substrate. Average sensitivities obtained through real time monitoring of the drain current I_D for (A) sensor 1; (B) sensor 2; (C) sensor 3.

A.5 Sensors on corning glass data measurements

Table A.1 - Summary of the results obtained for each tested sensor fabricated on corning glass substrate.

Corning Glass	Sensitivity [mV/pH][1] for constant I_{ref}	Sensitivity [uA/pH][1] for constant V_{ref}	Sensitivity [uA/pH][2]
Sensor 1	31.6 ± 3.5	17.2 ± 1.0	22.7 ± 0.1
Sensor 2	30.8 ± 6.9	16.7 ± 3.1	19.1 ± 1.3
Sensor 3	37.1 ± 5.4	21.2 ± 2.1	19.6 ± 0.6

[1] Sensitivity extracted from transfer characteristics; [2] Sensitivity extracted from real time monitoring.

A.6 Sensor batches capacitance dry tests

Table A.2 – Batch of sensors produced on Whatman paper substrate w/ coating: distribution of working sensors and corresponding capacitances.

	1	2	3	4	5	6	7	8	9	10
A	0.167	>1	0.164	0.156	>1	0.167	>1	0.234	>1	>1
B	0.181	0.187	0.178	0.176	0.191	0.182	0.190	0.190	0.202	>1
C	>1	0.189	>1	>1	0.205	>1	0.218	0.224	>1	>1
D	>1	0.190	0.174	>1	0.175	>1	0.224	>1	>1	>1
E	0.181	0.176	0.160	0.168	>1	0.214	0.256	0.283	0.258	>1

Working: 30 sensors Average: 0.195 nF Standard deviation: 0.031

Not working: 20 sensors

Table A.3 - Batch of sensors produced on CelSmartSense substrate w/ coating: distribution of working sensors and corresponding capacitances.

	1	2	3	4	5	6	7	8	9	10
A	>1	0.156	>1	0.160	0.172	0.168	0.185	0.185	0.190	>1
B	0.143	0.108	0.144	0.143	0.146	0.155	0.150	0.150	0.112	0.162
C	>1	0.111	0.18	0.166	0.166	0.155	0.150	0.142	0.131	0.162
D	0.140	0.155	0.144	0.108	0.108	0.147	0.150	0.126	0.124	0.166
E	>1	>1	>1	0.149	0.153	>1	0.114	0.473	>1	>1

Working: 40 sensors Average: 0.156 nF Standard deviation: 0.055

Not working: 10 sensors

Table A.4 - Batch of sensors produced on CelSmartSense substrate w/o coating: distribution of working sensors and corresponding capacitances.

	1	2	3	4	5	6	7	8	9	10
A	0.167	0.167	0.150	0.150	0.152	0.155	>1	>1	>1	0.130
B	0.177	0.182	0.157	0.203	0.157	0.257	0.174	0.185	>1	>1
C	0.164	0.270	0.270	0.159	0.152	0.157	0.149	0.26	0.14	>1
D	0.170	1.770	0.110	0.140	>1	>1	0.130	0.110	>1	>1
E	0.180	0.180	0.188	0.194	0.209	0.129	0.128	>1	0.220	>1

Working: 38 sensors Average: 0.215 nF Standard deviation: 0.265

Not working: 12 sensors

Table A.5 - Batch of sensors produced on PEN substrate: distribution of working sensors and corresponding capacitances.

	1	2	3	4	5	6	7	8	9	10
A	0.174	0.185	0.185	0.179	>1	0.180	0.190	0.190	0.216	>1
B	0.161	0.171	0.172	0.168	0.173	0.170	0.180	0.180	>1	>1
C	0.156	0.172	0.169	0.172	0.172	0.169	0.175	0.190	0.181	>1
D	0.170	0.187	0.174	0.168	0.169	0.174	0.178	>1	>1	>1
E	>1	0.210	0.196	0.188	0.190	>1	0.188	>1	0.218	>1

Working: 38 sensors Average: 0.180 nF Standard deviation: 0.013

Not working: 12 sensors

Table A.6 - Batch of sensors produced on Corning glass substrate: distribution of working sensors and corresponding capacitances.

	1	2	3	4	5	6	7	8	9	10
A	0.167	0.168	0.167	0.153	>1	0.154	0.15	0.183	0.226	0.200
B	0.161	0.166	0.172	0.168	0.173	0.169	>1	0.18	>1	>1
C	0.175	0.179	0.175	0.172	0.172	0.169	0.178	0.175	0.181	>1
D	0.170	0.180	0.175	0.200	0.165	>1	0.178	>1	0.181	>1
E	>1	>1	0.172	0.188	0.190	>1	0.188	0.188	0.198	0.200

Working: 39 sensors Average: 0.177 nF Standard deviation: 0.014

Not working: 11 sensors

2022

GABRIEL BARBOSA FÉLIX

PRODUCTION AND ELECTRICL CHARACTERISATION OF MICROSENSORS FOR MARINE MUTAGENS AD CARCINOGENS MONITORING

NOVA SCHOOL OF SCIENCE & TECHNOLOGY